An evaluation of ozone dry deposition in global scale chemistry climate models

C. Hardacre[1], O. Wild[1], and L. Emberson[2]

[1]Lancaster Environment Centre, Lancaster University, Lancaster, UK
[2]Stockholm Environment Institute, University of York, York, UK

Correspondence to: O. Wild (o.wild@lancaster.ac.uk)

Abstract

Dry deposition to the Earth's surface is an important process from both an atmospheric and biospheric perspective. Dry deposition controls the atmospheric abundance of many compounds as well as their input to vegetative surfaces, thus linking the atmosphere and biosphere. In many
[5] atmospheric and Earth system models it is represented using "resistance in series" schemes developed in the 1980s. These methods have remained relatively unchanged since their development and do not take into account more recent understanding of the underlying processes that have been gained through field and laboratory based studies. In this study we compare dry deposition of ozone across 15 models which contributed to the TF HTAP model intercomparison
[10] to identify where differences occur. We compare modelled dry deposition of ozone to measurements made at a variety of locations in Europe and North America, noting differences of up to a factor of two but no clear systematic bias over the sites examined. We identify a number of measures that are needed to provide a more critical evaluation of dry deposition fluxes and advance model development.

[15] 1 Introduction

Ozone is a significant trace gas constituent in the troposphere. The two main sources of tropospheric ozone are transport from the stratosphere and in situ chemical production via the oxidation of hydrocarbons and CO in the presence of nitrogen oxides (NO_x) (Crutzen, 1974; Liu et al., 1980; Atkinson, 2000). Tropospheric O_3, in addition to being a greenhouse gas
[20] (IPCC, 2013), is the primary driver of chemical oxidation in the troposphere as a source of OH radicals (e.g., Prather and Ehhalt, 2001) and is also a potent pollutant in its own right (The Royal Society, 2008).

Elevated concentrations of O_3 in the troposphere are detrimental to the human respiratory system and to plant health (e.g., WHO, 2005; Ashmore, 2005; The Royal Society,
[25] 2008; Fowler et al., 2009; Anenberg et al., 2010; Ainsworth et al., 2012; Emberson et al., 2013; Simpson et al., 2014) as it is a strong oxidant. Anenberg et al. (2010) estimated that anthro-

pogenic O_3 pollution was associated with 0.7 ± 0.3 million global deaths annually in the year 2000. It also has impacts on global agricultural production (Van Dingenen et al., 2009; Avnery et al., 2011a, b), with losses from three major crops estimated to be 11–18 billion USD_{2000} annually in the year 2000 (Avnery et al., 2011a) and projected to rise to 12–35 billion USD_{2000} in the year 2030 (Avnery et al., 2011b). However, the role of O_3 in future climate scenarios is not straightforward. The effect of O_3 on crop production between 2000 and 2050 may either exacerbate or offset the effects of climate change depending on scenario, crop type and region (Tai et al., 2014).

Ozone is primarily removed from the troposphere by chemical destruction and dry deposition to the Earth's surface. Dry deposition processes account for about 25 % of the total O_3 removed from the troposphere (Lelieveld and Dentener, 2000). Because it occurs at the Earth's surface–atmosphere interfaces, dry deposition constrains both the near surface O_3 concentration and the input of O_3 to surface ecosystems. In rural areas, dry deposition to terrestrial surfaces drives the diurnal variation in surface O_3 (Simpson, 1992). Further, for a reactive and polluting compound such as ozone, understanding dry deposition processes is particularly important for assessing impacts on terrestrial ecosystems where O_3 induced damage to vegetation may affect the hydrological cycle and key biogeochemical cycles, including those of carbon and nitrogen.

Dry deposition of O_3 to the terrestrial Earth surface is highly dependent on land cover. Deposition to non-vegetated surfaces is generally slower than deposition to vegetated surfaces (Wesely and Hicks, 2000) and the latter process varies according to plant species and seasonal changes in leaf area index (LAI). At vegetated surfaces, 30–90 % of O_3 dry deposition occurs via the stomata (Fowler et al., 2001; Cieslik, 2004; Fowler et al., 2009) and is controlled by stomatal conductance, which varies according to species and meteorological conditions. It is uptake of O_3 through the stomata that results in damage to plant tissues, which are subsequently exposed to the highly reactive O_3, negatively impacting plant health (e.g., Reich and Amundson, 1985; Fowler et al., 2001).

The strong link between dry deposition, the atmosphere and land cover means that this process is also subject to feedbacks from changes in climate, land use and air pollution (Ainsworth et al., 2012; Fuhrer, 2009; Sitch et al., 2007; Arneth et al., 2010; Ganzeveld et al.,

2010; Wu et al., 2012; Hollaway, 2012; Hardacre et al., 2013). For example, increasing atmospheric CO_2 has been shown to affect tropospheric O_3 as a result of changes in stomatal conductance (Sitch et al., 2007). However, despite the importance of dry deposition processes, they are some of the most uncertain and poorly constrained aspects of the tropospheric O_3 budget (Wild, 2007). This uncertainty arises from the complexity and heterogeneity in dry deposition processes which depend on meteorological conditions and the characteristics of the surface, along with a paucity of long term observation data sets for many land cover classes, including oceans, tropical forests and deserts.

Global chemistry transport models (CTMs) or chemistry climate models (CCMs) are needed to study O_3 at a global scale. Uncertainty in dry deposition arises partly from it occurring at sub-grid scales and because the process is heavily parameterized in models (Giannakopoulos et al., 1999; Wesely and Hicks, 2000; Fowler et al., 2009). The global O_3 dry deposition sink is estimated from a wide range of modelling studies to be about $1000\,\mathrm{Tg\,yr^{-1}}$ (Stevenson et al., 2006; Wild, 2007; Young et al., 2013). Of this, approximately one third is deposited to the oceans (Ganzeveld et al., 2009).

Many global scale CTMs parameterize dry deposition using the resistance in series approach developed by Wesely (1989) with some modifications (e.g., Wang et al., 1998; Ganzeveld and Lelieveld, 1995; ValMartin et al., 2014). This scheme is well characterized and has been previously reviewed, e.g. by Wesely and Hicks (2000); Fowler et al. (2009). The Wesely scheme does not, however, take into account newer understanding of dry deposition processes that has been gained from more recent measurement studies. Notably the importance of surface wetness, soil moisture, vapour pressure deficit and the role of stomatal versus non-stomatal uptake have been clearly demonstrated (Fowler et al., 2009). The latter is of particular importance for assessing the impact of O_3 on plants, as it is the uptake of O_3 through the stomata that results in damage to plant tissues.

Comparatively recent process models such as DO3SE (Emberson et al., 2000b, a, 2001; Buker et al., 2007), which was developed to estimate stomatal ozone flux, do parameterize the effect of soil water deficit and vapour pressure deficit on stomatal conductance. DO3SE has

4

recently been included in the EMEP model (Simpson et al., 2012) but these developments have not generally been implemented in global scale models.

In this study we conduct the first global scale assessment of O_3 dry deposition across a wide range of CTMs and CCMs. While dry deposition has been studied in detail in individual models (e.g., Tuovinen et al., 2004, 2009; Zhang et al., 2002) no general comparative evaluation has been performed across a wider range of models to explore model differences or weaknesses. Here, we identify the main differences between models and highlight the diagnostics that would be required from future studies to provide better constrints on O_3 dry deposition at the global scale. We use O_3 dry deposition fluxes from a subset of 15 models that contributed to the model intercomparison coordinated by the Task Force on Hemispheric Transport of Air Pollution (TF HTAP) (Fiore et al., 2009). Results from these models have been used to study nitrogen and sulfur deposition (Sanderson et al., 2008; Dentener et al., 2006) as well as tropospheric ozone (Stevenson et al., 2006) at the global scale, but an assessment of ozone dry deposition has not previously been undertaken.

We describe the methods used to process the model data in Sect. 2. The analysis of modelled O_3 dry deposition is shown in Sects. 3.1 and 3.2. We analyse O_3 deposition fluxes partitioned to land cover classes to evaluate the driving factors for variation in O_3 dry deposition that are associated with land cover across the model ensemble in Sect. 4. Finally, we compare modelled O_3 deposition fluxes to measurements in Sect. 5.

2 Methods

Ozone dry deposition fluxes were diagnosed and archived from 15 of the global chemistry transport models that participated in the TF HTAP modelling intercomparison project (for further details see http://www.htap.org). These models and the main differences between them are detailed in Sanderson et al. (2008), Dentener et al. (2006) and Stevenson et al. (2006). Average monthly O_3 dry deposition fluxes were taken from the TF HTAP control run (the "SR1 experiment") which was driven by meteorological fields for the year 2001. Note that the diurnal variation in deposition fluxes is not available from the TF HTAP results, so we focus our analy-

sis on monthly fluxes. The models used in this study are summarized in Table 1 and more detail on the deposition schemes and land cover are given in the Supplementary information.

In most of the models dry deposition of gases was represented using the resistance in series scheme described by Wesely (1989) or a modified version of this scheme. In this type of scheme the dry deposition velocity is determined from Eq. (1):

$$V_d = (R_a + R_b + R_c)^{-1} \tag{1}$$

where the terms R_a, R_b and R_c represent the aerodynamic resistance, quasi-laminar layer resistance and canopy surface resistance. Although this method is practical, the properties of the atmosphere and surface can be oversimplified (Wesely and Hicks, 2000). The R_c term may differ considerably between models depending on how individual surface resistance terms (e.g. stomatal resistance, R_{stom}, and mesophyll resistance, R_m) are represented (Wesely and Hicks, 2000). The original dry deposition module developed by Wesely (1989) described seven surface resistance terms for 11 land use types and five seasonal categories, but these may be mapped to the native land cover classes in the models differently.

The horizontal resolution of the different models ranged from $1° \times 1°$ to $10° \times 10°$, averaging approximately $3° \times 3°$. Ozone dry deposition fluxes from all models were therefore regridded to a common horizontal resolution of $3° \times 3°$ to enable ensemble means and standard deviations to be calculated for each grid box.

To account for first order variation in the simulated O_3 dry deposition fluxes arising from model differences in surface O_3, dry deposition velocities were also compared. Modelled deposition velocites are not available from the TF HTAP archive so these were calculated from Eq. (2):

$$V_d = F_{O_3}/C_{O_3} \tag{2}$$

where F_{O_3} and C_{O_3} are the simulated dry deposition flux and surface O_3 concentration layer respectively. These mean dry deposition velocities are O_3-weighted and thus do not account for diurnal variations in surface O_3 or O_3 flux, which are not available for this study, or for indirect variations in flux arising from the feedback between surface O_3 and its deposition, which limits

6

the fluxes when velocities are large. However, variation as a result of these processes is likely to be small compared with the variation in surface O_3.

To better characterise sources of variation in O_3 dry deposition between models the fluxes were partitioned to different land cover classes (LCCs). Modelled O_3 dry deposition is only available as a monthly average flux per grid cell so it was necessary to repartition the fluxes for different land classes. The repartitioned fluxes were then used to determine deposition velocities to individual land cover classes. The land cover schemes used in the TF HTAP models differ in their degree of classification, with some schemes including as many as 17 LCCs and others as few as five. The land cover schemes from individual models were not available for this study, so we apply two common schemes to all models. Ozone dry deposition fluxes for individual LCCs were determined by summing fluxes over grid cells, i, scaled by the fractional area, f, for that land cover class, c, see Eq. (3). Total O_3 deposition per LCC was determined globally over all grid cells and by latitude by summing over separate latitude bands.

$$F_c = \frac{\sum_i F_i \cdot A_i \cdot f_{i,c}}{\sum_i A_i} \tag{3}$$

The modelled O_3 dry deposition fluxes were compared to observed dry deposition fluxes from several sites, primarily located in Europe and North America. Seven of these data sets covered periods of more than a year and detailed comparisons between the modelled and observed O_3 dry deposition fluxes were made at these sites. Shorter term measurements were made at a number of other sites. The measurement sites are described in greater detail in Sect. 5.1.

To compare measured fluxes with the modelled average monthly O_3 dry deposition fluxes we focussed on studies that reported an average O_3 dry deposition flux or where long term average O_3 dry deposition fluxes data was independently made available for this study. We focus on datasets that include a full seasonal cycle so that we can explore how well the models resolve the large contrasts in O_3 dry deposition between summer and winter. We also compare the measured O_3 dry deposition fluxes with modelled fluxes repartitioned for the land cover classes in the corresponding grid cell. The flux to each land cover class was determined assuming that the ratio of the fluxes in the grid cell was the same as that around the corresponding latitude band.

7

This approach to repartitioning fluxes for individual LCCs was tested using a single model, the FRSGC/UCI CTM (Wild and Prather, 2000), where land cover specific fluxes were explicitly diagnosed. The repartitioned fluxes were found to be in reasonable agreement with the explicitly diagnosed fluxes, typically within about 10 % over the globe, and within 20 % for all
5   nine land cover classes considered. This gives an indication of the level of uncertainty associated with this simple partitioning approach.

We also compared the modelled monthly average O_3 dry deposition fluxes to data from the Clean Air Status and Trends Network (CASTNET, http://epa.gov/castnet/javaweb/index.html). As CASTNET deposition fluxes are derived using modelled deposition velocities rather than
10 directly measured fluxes, we discuss the results separately from our comparison with fluxes measured at European and North American sites. Hourly surface O_3 measurements and derived O_3 dry deposition velocities (Clarke et al., 1997; Finkelstein et al., 2000) are available for 96 sites across North America. We determined the monthly average surface O_3 and O_3 deposition velocity at each site and calculated the monthly average deposition flux. The data were
15 grouped by land cover class according to the site descriptions, and sites classified as forest, grassland, crop and shrub/desert are included here.

3   Results and discussion

3.1   Global variation in O_3 dry deposition

Annual global O_3 dry deposition fluxes from the 15 TF HTAP models are summarised in Ta-
20 ble 1, and the seasonal cycles are shown in Fig. 1 for three distinct latitude bands. The modelled annual global deposition fluxes ranged between 818–1258 Tg yr^{-1} across the models with an ensemble mean ($\pm 1\sigma$) of 978 ± 127 Tg yr^{-1}. This is very similar to that reported in previous modelling studies, including 949 ± 222 Tg yr^{-1} from 17 independent studies between 2000 and 2004 (Wild, 2007), 1003 ± 200 Tg yr^{-1} from 21 models contributing to the ACCENT model in-
25 tercomparison (Stevenson et al., 2006) and 1094 ± 241 Tg yr^{-1} from six models contributing to the recent ACCMIP intercomparison (Young et al., 2013). In these studies 9 out of 29 models in

Wild (2007), 9 out of 21 models in Stevenson et al. (2006) and 3 out of 6 models in Young et al. (2013) were similar to those used in this study.

Monthly O_3 deposition varied by an average of $38 \pm 6 \, \text{Tg month}^{-1}$ across the model ensemble, see Table 1. On average dry deposition velocities varied by $0.09 \pm 0.02 \, \text{cm s}^{-1}$ per month. The average relative standard deviations (RSD) for total monthly dry deposition and average monthly deposition velocity are 14% and 20%. The smaller RSD for total monthly deposition indicates that differences in surface O_3 compensate for some of the differences in O_3 dry deposition velocity between the models, i.e. that the O_3 deposition velocity is more different across the models than the O_3 deposition flux.

The original Wesely scheme describes a limited seasonality for surface resistance with smaller resistances to vegetated surfaces in spring and summer (Wesely, 1989). In this study the models agree well on the timing of the seasonal cycles in dry deposition in the Northern Hemisphere (NH), Tropics and the Southern Hemisphere (SH) (Fig. 1). Differences in the seasonality may arise from differences in meteorology or in surface vegetation cover. The effect of the latter is discussed further in Sect. 4.

Figure 1 shows that O_3 dry deposition is greatest in the Tropics and in the NH during the growing season. For all the HTAP models the most well-defined seasonal cycle in O_3 dry deposition occurs in the Northern Hemisphere with maximum and minimum deposition during the NH summer and winter respectively. In contrast the seasonality in the Tropics and Southern Hemisphere is much less pronounced. The average RSD in monthly total deposition over the models (NH=21%, Tropics=15% and SH=32%) is smaller than the average RSD in monthly average deposition velocity in the NH (31%), Tropics(21%) and SH (36%), again highlighting the compensation between surface O_3 and deposition velocity between the models in these regions.

3.2 Latitudinal variation in O_3 dry deposition

The latitudinal distribution of total annual O_3 dry deposition is shown for the model ensemble in Fig. 2. The O_3 dry deposition is greatest between $30°\,\text{S}$–$45°\,\text{N}$, with an average flux of 20–$37 \, \text{Tg yr}^{-1}$ per $3°$ latitude band, and the RSD over the models is relatively uniform at 15–20%.

9

In contrast, there are greater differences in dry deposition velocity between the models. Five models show a peak in deposition velocity at $0°$–$15°$ S. These models included a tropical forest or broadleaf evergreen forest land cover class, but were not the only models to do so. The RSD in the dry deposition velocity was generally between 30% and 35% at mid-latitudes.

The seasonality in the dry deposition flux is shown for Feburary and August in Figure 2 to highlight both the temporal and spatial variability in deposition. In February, O_3 dry deposition is greatest at $0°$–$30°$ N, driven by higher surface O_3 and LAI in this region, and the deposition velocities are fairly uniform between $30°$ N–$30°$ S. In August, peak deposition shifts northward to $30°$ N–$45°$ N, but peak dry deposition velocites occur further north, (approx. $55°$ N–$65°$ N) further indicating that high summertime O_3 dry deposition in the NH is driven by both increased LAI in the growing season and by high summertime surface O_3. (Stevenson et al., 2006; Fiore et al., 2009; Young et al., 2013). A second peak in O_3 deposition, also mainly driven by high surface O_3, occurs at $0°$–$30°$ S and is associated with dry deposition to deciduous trees and grassland.

4 O_3 dry deposition to different land cover classes

The greatest variation in O_3 dry deposition occurs between $45°$ N–$30°$ S, i.e. where vegetated terrestrial land cover is primarily located. To investigate how land cover contributes to variation in O_3 dry deposition across the model ensemble, the fluxes were partitioned to different land cover classes (LCCs) as described in Sect. 2.

Because the native land cover schemes used in the TF HTAP models are not available for this study, data from Olson 1992 (available though: http://acmg.seas.harvard.edu/geos/, Loveland et al., 2000) and the Global Land Cover Facility (GLCF, available from: http://www.landcover.org/, De Fries and Townshend, 1994) are used. This results in some additional uncertainty in the partitioned fluxes, particularly in regions where landcover is very heterogeneous. However, by using two different land cover schemes for partitioning fluxes across the model ensemble, we gain a clearer picture of the sensitivity of simulated O_3 dry deposition to land cover.

The Olson 1992 data set describes fractional grid cell coverage for 74 LCCs at $1° \times 1°$ resolution. These 74 LCCs were mapped to the 11 Wesely LCCs described in Table 2. The resulting land cover data set is henceforth termed the "OW11" data set. The GLCF data set describes grid cell coverage for 14 LCCs at $1° \times 1°$ resolution, but provides only the dominant LCC in each grid cell. Both data sets were regridded to the same $3° \times 3°$ resolution as the model output. The OW11 and GLCF LCCs and their global coverage are summarized in Table 2.

4.1 Variation in O_3 dry deposition fluxes at homogeneous grid cell locations

Variation in O_3 dry deposition velocity to individual LCCs was initially compared at $3°$ grid cells that were dominated by a single land cover class in the OW11 data set. Monthly O_3 dry deposition velocities were averaged over all grid cells with 100% coverage of a single LCC. Maps of these grid cells are provided in the Supplement. In taking this approach, we remove some of the uncertainty associated with using non-native land cover data, as models are likely to be reasonably consistent in their land cover across these regions. This analysis reveals the variability in O_3 dry deposition velocities to different LCCs across the ensemble. Urban and wetland LCCs were not considered here as their global coverage is small (see Table 2).

Figure 3 shows that seasonality in O_3 dry deposition velocities for the terrestrial vegetated LCCs agree well across the model ensemble. The only exception is one coarse resolution model which did not include any seasonal variation in O_3 dry deposition. The magnitude of the dry deposition velocities varies by 0.002–$0.25\,\mathrm{cm\,s^{-1}}$ across the model ensemble, with greatest variation occurring during the NH growing season for all terrestrial vegetated LCCs except tropical forest. O_3 dry deposition to tropical forest was not seasonal and variation across the ensemble was about $0.3\,\mathrm{cm\,s^{-1}}$ throughout the year (see Fig. 3c). At non-vegetated LCCs (oceans, snow/ice and deserts) the variation in O_3 dry deposition velocity across the ensemble was small.

The absence of seasonality in O_3 dry deposition velocity to tropical forests was likely due to relatively uniform annual LAI compared to other LCCs, such as coniferous forest, deciduous forest, agricultural cropland and tundra, where there are large differences in LAI between the growing and non-growing seasons. Different representation of LAI acorss the models is therefore likely to drive part of the observed greater spread in O_3 dry deposition over the models

11

during the NH growing season for coniferous forest, deciduous forest, agricultural cropland and tundra.

For deciduous forest and agricultural cropland high summertime O_3 dry deposition velocities were observed for two models. These models may either specify relatively high deposition velocites to these land cover classes, or classify and distribute land cover very differently to the other models. Diagnosing land cover specific dry deposition fluxes and velocities would allow for a more detailed analysis of the drivers of these differences between models.

4.2 Variation in total O_3 dry deposition to land cover classes

Figure 4 shows the total O_3 deposition to LCCs described in the OW11 and GLCF land cover data sets. The largest total flux of O_3 is to the oceans, which remove an average of $361 \, \mathrm{Tg} \, O_3 \, \mathrm{yr}^{-1}$, and this is followed by grasslands and deciduous trees which remove 207 and $142 \, \mathrm{Tg} \, O_3 \, \mathrm{yr}^{-1}$ respectively, based on fluxes partitioned to the OW11 data set. Partitioning to the GCLF data set gives a broadly similar picture, with oceans, wooded grassland and grassland responsible for fluxes of $319 \, \mathrm{Tg} \, O_3 \, \mathrm{yr}^{-1}$, $131 \, \mathrm{Tg} \, O_3 \, \mathrm{yr}^{-1}$ and $107 \, \mathrm{Tg} \, O_3 \, \mathrm{yr}^{-1}$ respectively.

Deciduous forest is not classified uniquely in the GCLF data set, and the corresponding area is predominantly considered as wooded grassland, broad leaf evergreen forest and broad leaf deciduous forest. The greater average O_3 dry deposition to broad leaf evergreen forest (BE) compared with tropical forest, $75 \, \mathrm{Tg} \, O_3 \, \mathrm{yr}^{-1}$ and $20 \, \mathrm{Tg} \, O_3 \, \mathrm{yr}^{-1}$ respectively, reflects the larger area for BE than tropical forest in OW11 (see Table 2). The average flux to other LCCs, e.g. crops and coniferous forest were broadly similar for the two land cover data sets.

Figure 4 clearly shows that total global O_3 deposited to oceans is both large and highly variable across the different models. Deposition to oceans is 250–$591 \, \mathrm{Tg} \, \mathrm{yr}^{-1}$ using the OW11 data set (209–$538 \, \mathrm{Tg} \, \mathrm{yr}^{-1}$ using the GCLF data set), representing a range of about $335 \, \mathrm{Tg} \, \mathrm{yr}^{-1}$ across the ensemble. The geographical distribution of O_3 dry deposition fluxes to the oceans indicates that differences between the models are spatially uniform. The range in total O_3 deposition to the other LCCs that are large O_3 sinks, e.g deciduous trees and grassland (OW11) and wooded grassland and BE (GCLF), is 70–$100 \, \mathrm{Tg} \, \mathrm{yr}^{-1}$.

12

The lower panels in Fig. 4 show that the variation in the average deposition velocity to oceans is small in absolute terms, $< 0.1\,\mathrm{cm\,s^{-1}}$. However, integrating these small differences over the large global area of ocean leads to large differences in total deposition. The sensitivity of surface O_3 to small variations in dry deposition velocity over the oceans was also reported by Ganzeveld et al. (2009), who found that surface O_3 differed by up to 60% when the O_3 dry deposition velocity was varied between 0.01 and $0.05\,\mathrm{cm\,s^{-1}}$. Improved characterization of deposition velocities over the ocean, building on the work of Ganzeveld et al. (2009) and Helmig et al. (2012) would therefore make a substantial contribution to reducing the uncertainty in total global O_3 dry deposition. Further, it is important to constrain the absolute deposition velocities for other LCCs that cover a large area, e.g. for grassland and to describe spatial variation in O_3 dry deposition better, e.g. with more descriptive land cover data sets.

Model differences are particularly evident for tropical forest where the range in average O_3 dry deposition velocity is $0.25\,\mathrm{cm\,s^{-1}}$. Tropical forest is not explicitly defined in some of the models used in this study, or in the original Wesely scheme, so it is apparent that a range of O_3 deposition velocities have been applied in these areas across the models. This has less impact for the O_3 dry deposition budget using the OW11 data set, where the tropical forest area is relatively small, but is a larger source of uncertainty when using the GCLF data set. It is important to include a well constrained O_3 dry deposition velocity and global area for tropical forests as observed mean daytime maximum velocities of $2.3\,\mathrm{cm\,s^{-1}}$ (Rummel et al., 2007) suggest that they are an effective O_3 sink.

This comparison highlights the importance of well constrained O_3 deposition velocities, particularly over water where small differences result in large discrepancies in total O_3 deposition, but also to tropical forests. The importance of land cover classification within models is also emphasized. The differences in fluxes to tropical forests could be greatly reduced by including a specific O_3 deposition velocity for this LCC. The LCC distribution is also shown to be important. For example, the tropical forest and broadleaf evergreen LCCs in the OW11 and GCLF data sets cover 0.8 and 2.9 % respectively, partly as a result of the use of dominant vegetation types as a $1°$ scale in the latter data set. A high O_3 dry deposition velocity over these

13

two areas would yield different total deposition and could have very different impacts on local atmospheric chemistry and composition.

4.3 Seasonal variation in O_3 dry deposition to land cover classes

The differences in total O_3 dry deposition between the months with highest and lowest deposi-
tion, representing the seasonal amplitude, are shown in Fig. 5. The largest seasonal amplitudes are found for deciduous forests, coniferous forests, agricultural crop land, grassland and water in the OW11 data set. Similarly, they are found for coniferous evergreen (CE), mixed coniferous forest (MC), crop land, grassland, high latitude deciduous forest and woodland (HL) and oceans in the GCLF data set.

10 These differences in the seasonal amplitude of deposition to coniferous, agricultural and high latitude LCCs in both data sets are driven by differences in the seasonal amplitude in O_3 depo-
sition velocity, shown in the lower panels of Fig. 5. These LCCs also have the largest annual variation in LAI, which is represented differently in the different models, and this contributes to differences in the seasonal amplitude in total O_3 deposition. In contrast, the differences in
15 seasonal amplitude in total O_3 dry deposition for oceans, grassland and deciduous forest are likely due to the large areas covered by these LCCs as differences in the seasonal amplitude in O_3 dry deposition velocities for these LCCs is small.

This analysis shows that the amplitude of the seasonal cycle in O_3 dry deposition differs substantially across the models. This is particularly apparent for LCCs that are predominant
20 at northern mid to high latitudes (deciduous forests, coniferous forests, mixed forests, tundra, agricultural and cropland) and grasslands. The seasonal amplitude is expected to be large at northern mid and high latitudes where there is a well defined seasonal cycle in LAI and meteo-
rology. However, the range in seasonal amplitudes suggests that seasonality in vegetation (LAI, etc.) or meteorology is somewhat different within the various models, in agreement with our
25 findings in Sect. 4.1.

Comparison of Figs. 4 and 5 shows that differences in the seasonal amplitude of O_3 dry de-
position to individual LCCs across the models remain small compared to the differences in total deposition. However, improved constraints on the seasonal amplitude in fluxes to seasonally

dependent LCCs, e.g. through consideration of stomatal uptake as a function of environmental parameters, and more coherent representation of land cover and LAI across the models would contribute to a better representation of dry deposition.

5 Comparison with observed O_3 dry deposition fluxes

5.1 Long term measurements

Modelled O_3 deposition fluxes are compared with measured fluxes at seven locations where at least one year of data is available. The measurement sites are summarized in Table 3. Monthly average O_3 dry deposition fluxes were calculated at these sites and compared with model fluxes. Ozone fluxes were generally measured using the eddy covariance method or the aerodynamic flux gradient method (see references in Table 3). Uncertainty in O_3 fluxes determined using these methods is around 12% (Bauer et al., 2000; Muller et al., 2010). All seven sites are located in the Northern Hemisphere, and hence "summer", "winter" and "growing season" in the following sections refer to NH timings for these periods.

The modelled and observed monthly O_3 dry deposition fluxes are compared in Figs. 6 and 7. At each site the observed monthly fluxes were averaged across a number of years (the measurement period is indicated in Table 3) and the simulated monthly fluxes were averaged across the model ensemble. O_3 dry deposition velocities and surface O_3 concentrations were also compared at these sites. For each comparison, the seasonality and bias were assessed using the Pearson correlation coefficient and the line of best fit. The seasonality of the observed and modelled O_3 dry deposition fluxes are shown in more detail in Fig. 8 where the average monthly fluxes are shown for each year of measurements and for each model. Measurements from Harvard Forest in 2005 were not available between June and August and were exceptionally low in May, September and November for that year.

At Ulborg, Hyytiala, Harvard Forest, the citrus orchard and Blodgett Forest the correlation coefficients for the comparison between the observed and modelled O_3 dry deposition fluxes are greater than 0.85, indicating that the models are able to capture the seasonal cycle in O_3

15

dry deposition well at these sites. The lower correlation coefficients at Castel Porziano and Auchencorth Moss reflect a difference in the timing of the peak fluxes in summertime. Observed fluxes were greatest in April and May, whereas the models simulated peak fluxes in June, as shown in Fig. 8.

5 O_3 dry deposition fluxes and surface O_3 at Auchencorth Moss suggest that the early peak in O_3 dry deposition is driven by relatively high surface O_3 at this time. At Castel Porziano, surface O_3 concentrations in April and May are lower than in summertime suggesting that high dry deposition velocities drive the greater springtime fluxes at this site.

The slope of the best fit lines for the modelled and observed O_3 dry deposition fluxes lie
10 between 0.27 and 1.74 across the different measurement sites. Ozone dry deposition fluxes were underestimated at Ulborg, Auchencorth Moss and Blodgett Forest, and overestimated at Harvard Forest and Hyytiala. The best agreement between the modelled and observed fluxes was at the citrus orchard site, where the models slightly overestimated O_3 dry deposition through out the year, although it should be noted that only a single year of data was available for this
15 site. Although the number of sites is small, we do not find any clear systematic bias in O_3 dry deposition fluxes over the sites as a whole.

We find a greater discrepancy between the modelled and measured O_3 dry deposition fluxes in the growing season than in the winter months at all of the measurement sites except the citrus orchard. These biases do not appear to result from poor simulation of the seasonal cycle in the
20 surface O_3, as this is generally captured well. Rather, it appears that the seasonal amplitude in O_3 dry deposition fluxes is not represented well in the models. For example, at Blodgett Forest the observed fluxes during the growing season are 2–3 times greater than the modelled fluxes over the same period (Fig. 8g). In contrast, at Hyytiala, the modelled growing season fluxes are approximately twice as large as the observed fluxes (Fig. 8d).

25 Surface O_3 and its seasonal cycle are generally captured well by the models at all of the measurement sites. The correlation coefficients lie between 0.73 and 0.94 and the slopes range from 0.46 to 0.97. Consequently, the modelled dry deposition velocities do not match the measurement data better than the dry deposition fluxes, although there is less seasonal variation in the dry deposition velocities as the observed seasonal cycle in surface O_3 is captured well. This

16

indicates that biases in modelled O_3 dry deposition fluxes are due to the representation of dry deposition velocities rather than biases in surface O_3.

5.2 Partitioned modelled O_3 dry deposition fluxes

Comparing point observations with modelled O_3 dry deposition fluxes presents a number of
5 challenges. Measurement sites may not be representative of the model grid cell, and the grid cell may not provide an accurate representation of the land cover at the site. Figure 9 shows a comparison between observed fluxes and the modelled fluxes partitioned between the various LCCs located in the grid cell in which the measurement site was located. LCC coverage for the model grid cells was obtained from the OW11 land cover data set which described fractional
10 land cover.

It is clear that in some cases the LCC at the measurement site is not represented in the corresponding model grid cell. The Ulborg and Hyytiala measurement sites are situated in coniferous forests, but the OW11 data set does not include coniferous forest in the corresponding grid cells. The partitioned fluxes for deciduous forest and agricultural cropland at Ulborg, and for decid-
15 uous forest, agricultural cropland and water at Hyytiala are not found to be in better agreement with the observed O_3 dry deposition fluxes than the total modelled flux. Similarly, at Blodgett Forest in California, a deciduous forest site, the land cover classes are desert and grassland, and this partly explains the model underestimation of fluxes here.

At Auchencorth Moss, Harvard Forest and the citrus orchard there is better agreement in
20 LCCs between the OW11 data set and the measurement site. At these sites fluxes partitioned to more relevant LCCs are generally in better agreement with the observed fluxes. At the Californian citrus orchard the fluxes to cropland and deciduous forest fit the observed fluxes very well. At Auchencorth Moss, the flux partitioned to crop land is in slightly better agreement with the observations than that due to grassland. At Harvard Forest, the flux partitioned to deciduous
25 forest is higher than that observed, and the flux to coniferous forest is somewhat closer.

We have demonstrated that selecting an appropriate land cover class can lead to improved agreement between modelled and observed O_3 dry deposition fluxes, although this is not always the case. This analysis highlights the difficulties in comparing modelled fluxes with observa-

17

tions, particularly where an appropriate land cover class is unavailable. However, our findings suggest that future comparison of modelled and observed fluxes should be based on model-diagnosed fluxes to the most relevant land cover class within a grid cell using the native LCC scheme in the model, not merely total fluxes at the correct geographical location.

5.3 CASTNET sites

Modelled O_3 dry deposition fluxes, dry deposition velocity and surface O_3 were compared with average monthly values at 96 CASTNET sites grouped according to land cover class, see Fig. 10. The Pearson correlation coefficient and the slope of the line of best fit value are shown for the individual sites in the Supplementary information. The seasonal cycle in O_3 dry deposition flux is generally well represented by the models at the forest, grassland and crop sites with r^2 values generally greater than 0.8. However, at these sites the models tend to overestimate O_3 dry deposition fluxes by about 30 %. Conversely at the shrub and desert sites the models often underestimate the O_3 dry deposition fluxes and do not capture any seasonal variation well. Several, although not all, of these sites were situated in terrain classified as "complex" or "mountain top".

Comparison between the modelled and CASTNET O_3 dry deposition velocities and surface O_3 show that while surface O_3 is generally well represented in the models (as also seen in Fiore et al. (2009)), dry deposition velocities are represented less well. This suggests that the bias in modelled O_3 dry deposition fluxes is driven by bias in the modelled O_3 dry deposition velocity rather than bias in the modelled surface O_3. In particular, the seasonal cycle is not captured well, with modelled deposition velocities too high in the spring and autumn months, suggesting that the increase in O_3 dry deposition velocity from winter to summer occurs too soon.

It is not clear from this comparison alone what is driving the disparity between the modelled and the CASTNET O_3 dry deposition velocities. However, the differences are most pronounced for the forest and cropland LCCs. Changes in LAI during spring and summer are expected to be greatest for these LCCs, suggesting that this parameter is not well represented in these

18

global scale models. Diagnosis of LAI in future model studies would allow the influence of this variable to be determined more clearly.

5.4 Short term measurements

Modelled O_3 dry deposition fluxes were compared with observations at a number of sites where short term flux measurements are available, see Table 3. Figure 11 shows that agreement between the observed and modelled O_3 dry deposition fluxes are variable at these sites. At crop sites, the models generally overestimated fluxes to the maize crops, but underestimated fluxes at other crop locations. O_3 dry deposition fluxes are underestimated at the coniferous forest, but overestimated at the shrub locations.

The modelled and measured O_3 dry deposition fluxes agreed well at the tropical forest and oil palm sites in Malaysian Borneo, but less well at the Amazonian tropical forest sites. There was also less variation in O_3 dry deposition fluxes across the models at the Malaysian Borneo sites than at the Amazonian sites, possibly due to the large fraction of ocean in the Malaysian Borneo grid cell. Variation in the modelled O_3 dry deposition fluxes at the Amazonian sites is similar to that in the tropical forests shown in Fig. 3. The temporally and spatially limited scale of the measurement data makes it difficult to draw conclusions about model performance at tropical forest sites, but there does not appear to be systematic bias for this LCC.

The short term crop, coniferous forest, grass and shrub sites were all located in Europe and the models did not capture the range in O_3 dry deposition fluxes that were observed at these sites. However, the regional average observed flux over these sites ($7.9\,\mathrm{nmol\,m^{-2}\,s^{-1}}$) lies close to the range of the modelled fluxes ($5.8 \pm 2.1\,\mathrm{nmol\,m^{-2}\,s^{-1}}$) suggesting that there is no clear systematic bias in the modelled fluxes over this region.

It is likely that models are unable to capture the spatial variability in O_3 dry deposition at the European sites given the coarse grid resolution used here. The measurement sites span a range of heterogeneous land cover types, including natural and semi-natural vegetation as well as agricultural and urban areas, within a relatively small geographical region. This heterogeneity is not captured in the OW11 land cover data set, which assigns a similar combination of coniferous tree, deciduous tree, grassland and agricultural/crop land to grid cells in the Western European

region. There will be a similar lack of spatial resolution in the native land cover schemes in the models.

The short time scales over which these measurements were made renders it difficult to assess how well the models capture the seasonality at these sites. Measurements at Castel Porziano (Mediterranean pseudosteppe) and Burriana (citrus orchard) covered two different months in different years. At Burriana the difference in O_3 dry deposition fluxes between May and July is small, in agreement with observations in the Californian citrus orchard. At the Castel Porziano site there is a much greater difference between O_3 dry deposition fluxes observed in May and June in the different years, probably representing meteorological differences over the relatively short observation periods.

The comparison between these observations and the global scale models highlights the difficulty in comparing models with observations, especially in regions with very heterogeneous land cover such as Western Europe. This was also noted in the evaluation of the EMEP (Tuovinen et al., 2004, 2009) and AURUMS (Zhang et al., 2002) models. While a finer resolution global or regional-scale model may be able to capture the spatial variability in O_3 dry deposition observed here, better diagnosis of land cover specific fluxes would be valuable to identify the key weaknesses in current model deposition schemes. Previous evaluations of the EMEP and AURUMS models suggests that soil moisture deficit and parameterization of non stomatal fluxes represent key uncertainties in the dry deposition schemes implemented in regional scale models and are likely to contribute to the discrepancies between modelled and measured fluxes observed in this study. In addition, near surface and in canopy chemistry of O_3 (Chang et al., 2004; Wolfe et al., 2011) is not accounted for in the global scale models used in this study. These processes occur at small physical scales, but may contribute to differences between modelled and measured fluxes. Our comparison further highlights the need for spatially representative flux measurements over extended periods (ideally seasonal to annual periods) that are not greatly affected by the short-term variability in meteorology or vegetation properties.

20

6 Conclusions

This study provides the first analysis of O_3 dry deposition fluxes in global scale chemistry climate models. We identify regions where O_3 dry deposition differs substantially across an ensemble of 15 global models and show how land cover drives these differences. We also compare modelled O_3 dry deposition fluxes to observations at a range of measurement sites.

An initial assessment of O_3 dry deposition across latitudes shows that it is most variable between southern and northern mid-latitudes, and the extent of the variation across the models is dependent on the season. The greatest differences in total O_3 dry deposition across the models occur where deposition velocities and surface O_3 concentrations are highest. The particularly large differences in deposition at tropical latitudes are driven by a small number of models which simulate comparatively low surface O_3 in this region. These results indicate the need for better constraints of O_3 dry deposition during the growing season and at tropical latitudes.

To investigate the causes of the differences in dry deposition across the models, fluxes were partitioned to land cover class. We find that differences in O_3 dry deposition flux to oceans, driven by small absolute differences in dry deposition velocity, are the largest contributor to differences in the global O_3 deposition flux. Over continental regions, deposition to grasslands showed the greatest difference between models. Again, this was driven by relatively small absolute differences in deposition velocity integrated over the 8–9 % of the global surface area covered by grassland. Modelled O_3 dry deposition fluxes differed most over tropical forests, suggesting large differences in deposition velocity and the absence of this land cover class in some models. The magnitude of the deposition to oceans means that it is important for the global ozone budget that this term is constrained better. However, deposition to terrestrial ecosystems has important implications for many other components of the Earth system including carbon sequestration, hydrology and atmospheric composition.

This comparison of O_3 dry deposition partitioned to LCC demonstrates that differences in total O_3 dry deposition across the models could be greatly reduced by improved constraints on deposition velocities, particularly to oceans, grasslands and tropical forests. The importance of well constrained fluxes to oceans was noted by Ganzeveld et al. (2009) who found that small

differences in O_3 dry deposition flux could drive large differences in tropospheric O_3. Differences in O_3 deposition to grasslands or tropical forests will have a much smaller effect on the global tropospheric O_3 burden, but may significantly impact local atmospheric composition.

We highlight the degree of variation in ozone dry deposition that results from differences in the land cover classification used in the different global scale models. Some models use very limited land cover schemes with as few as five LCCs, and this may be a particular problem for simpler Earth System Models where vegetation processes are explicitly simulated online. This results in some LCCs, e.g. tropical forest, being omitted altogether. Further, deposition flux measurements are available from a relatively limited range of land cover classes, so differences in mapping these to the native LCC scheme leads to differing global coverage and deposition in different models. This may lead to substantial differences in local surface O_3 even though the global O_3 burden is not greatly affected. Tropical forests are important regions for atmospheric processing, for example, and observations have shown that O_3 dry deposition is relatively fast in these locations. Application of a generic deciduous forest or forest to this land cover therefore results in underestimation of O_3 deposition fluxes and a systematic bias in the chemical environment here.

We do not have sufficient data from the HTAP model study to assess the impact of other biases which are likely to drive model differences in O_3 dry deposition. Biases in the diurnal cycle of deposition fluxes and partitioning between stomatal and non-stomatal fluxes are likely to be cumulative across large areas and may have a significant effect on global annual O_3 dry deposition. While global scale model intercomparison projects have not previously reported O_3 dry deposition at this level of detail, we recommend that future model comparisons request these additional flux diagnostics to allow deposition processes to be tested more thoroughly.

In this study we make the first assessment of O_3 dry deposition fluxes in global models against observations. The models generally simulate the seasonal variations in O_3 dry deposition fluxes well. While our comparison of modelled O_3 deposition fluxes with direct flux observations did not show a systematic bias, comparison with fluxes derived form CASTNET observations suggests that the models overestimate O_3 dry deposition fluxes over North America. In general, we find that the discrepancy between modelled and observed O_3 dry deposition

22

fluxes is driven by the modelled O_3 dry deposition velocity rather than by surface O_3, but this is not the case at all sites.

This comparison between the models and observations provides an initial set of metrics that can be used as a simple indicator of model performance. More critical testing of model perfor-
5 mance will require more detailed diagnostics of O_3 dry deposition, including fluxes partitioned by land cover class, stomatal and non-stomatal fluxes, and fluxes at higher temporal resolution to explore the diurnal behaviour. It will also be important to have long-term flux measurements, over at least a full seasonal cycle, from sites with land cover classes that are broadly representative of a wider region. Characterization of deposition velocities over a wide range of land cover
10 classes would be particularly valuable for refining the variables used in current model resistance schemes, including over the ocean where differences between models are large. These should allow us to place better constraints on this important term in the global O_3 budget.

The Supplement related to this article is available online at doi:10.5194/acpd-0-1-2015-supplement.

23

References

References

Ainsworth, E. A., Yendrek, C. R., Sitch, S., Collins, W. J., and Emberson, L. D.: The Effects of Tropospheric Ozone on Net Primary Productivity and Implications for Climate Change, Annual Review of Plant Biology, Vol 63, 63, 637–661, doi:10.1146/annurev-arplant-042110-103829, 2012.

Anenberg, S. C., Horowitz, L. W., Tong, D. Q., and West, J. J.: An Estimate of the Global Burden of Anthropogenic Ozone and Fine Particulate Matter on Premature Human Mortality Using Atmospheric Modeling, Environmental Health Perspectives, 118, 1189–1195, doi:10.1289/ehp.0901220, 2010.

Arneth, A., Harrison, S. P., Zaehle, S., Tsigaridis, K., Menon, S., Bartlein, P. J., Feichter, J., Korhola, A., Kulmala, M., O'Donnell, D., Schurgers, G., Sorvari, S., and Vesala, T.: Terrestrial biogeochemical feedbacks in the climate system, Nature Geoscience, 3, 525–532, doi:10.1038/ngeo905, 2010.

Ashmore, M. R.: Assessing the future global impacts of ozone on vegetation, Plant Cell and Environment, 28, 949–964, doi:10.1111/j.1365-3040.2005.01341.x, 2005.

Atkinson, R.: Atmospheric chemistry of VOCs and NOx, Atmospheric Environment, 34, 2063–2101, doi:10.1016/S1352-2310(99)00460-4, 2000.

Avnery, S., Mauzerall, D. L., Liu, J., and Horowitz, L. W.: Global crop yield reductions due to surface ozone exposure: 1. Year 2000 crop production losses and economic damage, Atmospheric Environment, 45, 2284–2296, doi:10.1016/j.atmosenv.2010.11.045, 2011a.

Avnery, S., Mauzerall, D. L., Liu, J., and Horowitz, L. W.: Global crop yield reductions due to surface ozone exposure: 2. Year 2030 potential crop production losses and economic damage under two scenarios of {O3} pollution, Atmospheric Environment, 45, 2297 – 2309, doi:http://dx.doi.org/10.1016/j.atmosenv.2011.01.002, 2011b.

Bauer, M. R., Hultman, N. E., Panek, J. A., and Goldstein, A. H.: Ozone deposition to a ponderosa pine plantation in the Sierra Nevada Mountains (CA): A comparison of two different climatic years, Journal of Geophysical Research-atmospheres, 105, 22 123–22 136, doi:10.1029/2000JD900168, 2000.

Bey, I., Jacob, D. J., Yantosca, R. M., Logan, J. A., Field, B. D., Fiore, A. M., Li, Q. B., Liu, H. G. Y., Mickley, L. J., and Schultz, M. G.: Global modeling of tropospheric chemistry with assimilated meteorology: Model description and evaluation, Journal of Geophysical Research-atmospheres, 106, 23 073–23 095, doi:10.1029/2001JD000807, 2001.

24

Buker, P., Emberson, L. D., Ashmore, M. R., Cambridge, H. M., Jacobs, C. M. J., Massman, W. J., Muller, J., Nikolov, N., Novak, K., Oksanen, E., Schaub, M., and de la Torre, D.: Comparison of different stomatal conductance algorithms for ozone flux modelling, Environmental Pollution, 146, 726–735, doi:10.1016/j.envpol.2006.04.007, 2007.

Chang, W. N., Heikes, B. G., and Lee, M. H.: Ozone deposition to the sea surface: chemical enhancement and wind speed dependence, Atmospheric Environment, 38, 1053–1059, doi:10.1016/j.atmosenv.2003.10.050, 2004.

Cieslik, S. and Labatut, A.: Ozone surface fluxes and stomatal activity, Proceedings of Eurotrac Symposium '96 - Transport and Transformation of Pollutants In the Troposphere, Vol 2: Emissions, Deposition, Laboratory Work and Instrumentation, 31, 177–184, 1997.

Cieslik, S. A.: Ozone uptake by various surface types: a comparison between dose and exposure, Atmospheric Environment, 38, 2409–2420, doi:10.1016/j.atmosenv.2003.10.063, 2004.

Clarke, J. F., Edgerton, E. S., and Martin, B. E.: Dry deposition calculations for the clean air status and trends network, Atmospheric Environment, 31, 3667–3678, doi:10.1016/S1352-2310(97)00141-6, 1997.

Collins, W., Stevenson, D., Johnson, C., and Derwent, R.: Tropospheric Ozone in a Global-Scale Three-Dimensional Lagrangian Model and Its Response to NOX Emission Controls, Journal of Atmospheric Chemistry, 26, 223–274, doi:10.1023/A:1005836531979, http://dx.doi.org/10.1023/A%3A1005836531979, 1997.

Collins, W. J., Derwent, R. G., Garnier, B., Johnson, C. E., Sanderson, M. G., and Stevenson, D. S.: Effect of stratosphere-troposphere exchange on the future tropospheric ozone trend, Journal of Geophysical Research-atmospheres, 108, 8528, doi:10.1029/2002JD002617, 2003.

Coyle, M., Nemitz, E., Storeton-West, R., Fowler, D., and Cape, J. N.: Measurements of ozone deposition to a potato canopy, Agricultural and Forest Meteorology, 149, 655–666, doi:10.1016/j.agrformet.2008.10.020, 2009.

Crutzen, P. J.: Photochemical Reactions Initiated By and Influencing Ozone In Unpolluted Tropospheric Air, Tellus, 26, 47–57, 1974.

De Fries, R. S. and Townshend, J. R. G.: Ndvi-derived Land-cover Classifications At A Global-scale, International Journal of Remote Sensing, 15, 3567–3586, 1994.

Dentener, F., Drevet, J., Lamarque, J. F., Bey, I., Eickhout, B., Fiore, A. M., Hauglustaine, D., Horowitz, L. W., Krol, M., Kulshrestha, U. C., Lawrence, M., Galy-Lacaux, C., Rast, S., Shindell, D., Stevenson, D., Van Noije, T., Atherton, C., Bell, N., Bergman, D., Butler, T., Cofala, J., Collins, B., Doherty, R., Ellingsen, K., Galloway, J., Gauss, M., Montanaro, V., Mueller, J. F., Pitari, G.,

Rodriguez, J., Sanderson, M., Solmon, F., Strahan, S., Schultz, M., Sudo, K., Szopa, S., and Wild, O.: Nitrogen and sulfur deposition on regional and global scales: A multimodel evaluation, Global Biogeochemical Cycles, 20, GB4003, doi:10.1029/2005GB002672, 2006.

Emberson, L. D., Ashmore, M. R., Cambridge, H. M., Simpson, D., and Tuovinen, J. P.: Modelling stomatal ozone flux across Europe, Environmental Pollution, 109, 403–413, doi:10.1016/S0269-7491(00)00043-9, 2000a.

Emberson, L. D., Wieser, G., and Ashmore, M. R.: Modelling of stomatal conductance and ozone flux of Norway spruce: comparison with field data, Environmental Pollution, 109, 393–402, doi:10.1016/S0269-7491(00)00042-7, 2000b.

Emberson, L. D., Ashmore, M. R., Simpson, D., Tuovinen, J. P., and Cambridge, H. M.: Modelling and mapping ozone deposition in Europe, Water Air and Soil Pollution, 130, 577–582, doi:10.1023/A:1013851116524, 2001.

Emberson, L. D., Kitwiroon, N., Beevers, S., Bueker, P., and Cinderby, S.: Scorched Earth: how will changes in the strength of the vegetation sink to ozone deposition affect human health and ecosystems?, Atmospheric Chemistry and Physics, 13, 6741–6755, doi:10.5194/acp-13-6741-2013, 2013.

Fan, S. M., Wofsy, S. C., Bakwin, P. S., Jacob, D. J., and Fitzjarrald, D. R.: Atmosphere-biosphere Exchange of Co2 and O3 In the Central-amazon-forest, Journal of Geophysical Research-atmospheres, 95, 16 851–16 864, doi:10.1029/JD095iD10p16851, 1990.

Fares, S., Park, J.-H., Ormeno, E., Gentner, D. R., McKay, M., Loreto, F., Karlik, J., and Goldstein, A. H.: Ozone uptake by citrus trees exposed to a range of ozone concentrations, Atmospheric Environment, 44, 3404–3412, doi:10.1016/j.atmosenv.2010.06.010, 2010.

Fares, S., Weber, R., Park, J.-H., Gentner, D., Karlik, J., and Goldstein, A. H.: Ozone deposition to an orange orchard: Partitioning between stomatal and non-stomatal sinks, Environmental Pollution, 169, 258–266, doi:10.1016/j.envpol.2012.01.030, 2012.

Fares, S., Savi, F., Muller, J., Matteucci, G., and Paoletti, E.: Simultaneous measurements of above and below canopy ozone fluxes help partitioning ozone deposition between its various sinks in a Mediterranean Oak Forest, Submitted to: Agricultural and Forest Meteorology, 2014.

Finkelstein, P. L., Ellestad, T. G., Clarke, J. F., Meyers, T. P., Schwede, D. B., Hebert, E. O., and Neal, J. A.: Ozone and sulfur dioxide dry deposition to forests: Observations and model evaluation, Journal of Geophysical Research-atmospheres, 105, 15 365–15 377, doi:10.1029/2000JD900185, 2000.

Fiore, A. M., Dentener, F. J., Wild, O., Cuvelier, C., Schultz, M. G., Hess, P., Textor, C., Schulz, M., Doherty, R. M., Horowitz, L. W., MacKenzie, I. A., Sanderson, M. G., Shindell, D. T., Stevenson,

D. S., Szopa, S., Van Dingenen, R., Zeng, G., Atherton, C., Bergmann, D., Bey, I., Carmichael, G., Collins, W. J., Duncan, B. N., Faluvegi, G., Folberth, G., Gauss, M., Gong, S., Hauglustaine, D., Holloway, T., Isaksen, I. S. A., Jacob, D. J., Jonson, J. E., Kaminski, J. W., Keating, T. J., Lupu, A., Marmer, E., Montanaro, V., Park, R. J., Pitari, G., Pringle, K. J., Pyle, J. A., Schroeder, S., Vivanco, M. G., Wind, P., Wojcik, G., Wu, S., and Zuber, A.: Multimodel estimates of intercontinental source-receptor relationships for ozone pollution, Journal of Geophysical Research-atmospheres, 114, D04 301, doi:10.1029/2008JD010816, 2009.

Fowler, D., Flechard, C., Cape, J. N., Storeton-West, R. L., and Coyle, M.: Measurements of ozone deposition to vegetation quantifying the flux, the stomatal and non-stomatal components, Water Air and Soil Pollution, 130, 63–74, doi:10.1023/A:1012243317471, 2001.

Fowler, D., Pilegaard, K., Sutton, M. A., Ambus, P., Raivonen, M., Duyzer, J., Simpson, D., Fagerli, H., Fuzzi, S., Schjoerring, J. K., Granier, C., Neftel, A., Isaksen, I. S. A., Laj, P., Maione, M., Monks, P. S., Burkhardt, J., Daemmgen, U., Neirynck, J., Personne, E., Wichink-Kruit, R., Butterbach-Bahl, K., Flechard, C., Tuovinen, J. P., Coyle, M., Gerosa, G., Loubet, B., Altimir, N., Gruenhage, L., Ammann, C., Cieslik, S., Paoletti, E., Mikkelsen, T. N., Ro-Poulsen, H., Cellier, P., Cape, J. N., Horvath, L., Loreto, F., Niinemets, U., Palmer, P. I., Rinne, J., Misztal, P., Nemitz, E., Nilsson, D., Pryor, S., Gallagher, M. W., Vesala, T., Skiba, U., Brueggemann, N., Zechmeister-Boltenstern, S., Williams, J., O'Dowd, C., Facchini, M. C., de Leeuw, G., Flossman, A., Chaumerliac, N., and Erisman, J. W.: Atmospheric composition change: Ecosystems-Atmosphere interactions, Atmospheric Environment, 43, 5193–5267, doi:10.1016/j.atmosenv.2009.07.068, 2009.

Fowler, D., Nemitz, E., Misztal, P., Di Marco, C., Skiba, U., Ryder, J., Helfter, C., Cape, J. N., Owen, S., Dorsey, J., Gallagher, M. W., Coyle, M., Phillips, G., Davison, B., Langford, B., MacKenzie, R., Muller, J., Siong, J., Dari-Salisburgo, C., Di Carlo, P., Aruffo, E., Giammaria, F., Pyle, J. A., and Hewitt, C. N.: Effects of land use on surface-atmosphere exchanges of trace gases and energy in Borneo: comparing fluxes over oil palm plantations and a rainforest, Philosophical Transactions of the Royal Society B-biological Sciences, 366, 3196–3209, doi:10.1098/rstb.2011.0055, 2011.

Fuhrer, J.: Ozone risk for crops and pastures in present and future climates, Naturwissenschaften, 96, 173–194, doi:10.1007/s00114-008-0468-7, 2009.

Ganzeveld, L. and Lelieveld, J.: Dry Deposition Parameterization In A Chemistry General-circulation Model and Its Influence On the Distribution of Reactive Trace Gases, Journal of Geophysical Research-atmospheres, 100, 20 999–21 012, doi:10.1029/95JD02266, 1995.

Ganzeveld, L., Helmig, D., Fairall, C. W., Hare, J., and Pozzer, A.: Atmosphere-ocean ozone exchange: A global modeling study of biogeochemical, atmospheric, and waterside turbulence dependencies, Global Biogeochemical Cycles, 23, GB4021, doi:10.1029/2008GB003301, 2009.

Ganzeveld, L., Bouwman, L., Stehfest, E., van Vuuren, D. P., Eickhout, B., and Lelieveld, J.: Impact of future land use and land cover changes on atmospheric chemistry-climate interactions, Journal of Geophysical Research-atmospheres, 115, D23 301, doi:10.1029/2010JD014041, 2010.

Gerosa, G., Derghi, F., and Cieslik, S.: Comparison of different algorithms for stomatal ozone flux determination from micrometeorological measurements, Water Air and Soil Pollution, 179, 309–321, doi:10.1007/s11270-006-9234-7, 2007.

Giannakopoulos, C., Chipperfield, T. P., Law, K. S., and Pyle, J. A.: Validation and intercomparison of wet and dry deposition schemes using Pb-210 in a global three-dimensional off-line chemical transport model, Journal of Geophysical Research-atmospheres, 104, 23 761–23 784, doi:10.1029/1999JD900392, 1999.

Hardacre, C. J., Palmer, P. I., Baumanns, K., Rounsevell, M., and Murray-Rust, D.: Probabilistic estimation of future emissions of isoprene and surface oxidant chemistry associated with land-use change in response to growing food needs, Atmospheric Chemistry and Physics, 13, 5451–5472, doi:10.5194/acp-13-5451-2013, 2013.

Hauglustaine, D. A., Hourdin, F., Jourdain, L., Filiberti, M. A., Walters, S., Lamarque, J. F., and Holland, E. A.: Interactive chemistry in the Laboratoire de Meteorologie Dynamique general circulation model: Description and background tropospheric chemistry evaluation, Journal of Geophysical Research-atmospheres, 109, D04 314, doi:10.1029/2003JD003957, 2004.

Helmig, D., Lang, E., Bariteau, L., Boylan, P., Fairall, C., Ganzeveld, L., Hare, J., Hueber, J., and Pallandt, M.: Atmosphere-ocean ozone fluxes during the TexAQS 2006, STRATUS 2006, GOMECC 2007, GasEX 2008 and AMMA 2008 cruises, Journal of Geophysical Research, 117, D015 955, 2012.

Hollaway, M. J.: Modelling Interactions Between Vegetation and Tropospheric Ozone, Ph.D. thesis, University of Leeds, 2012.

Horowitz, L. W., Walters, S., Mauzerall, D. L., Emmons, L. K., Rasch, P. J., Granier, C., Tie, X., Lamarque, J.-F., Schultz, M. G., Tyndall, G. S., Orlando, J. J., and Brasseur, G. P.: A global simulation of tropospheric ozone and related tracers: Description and evaluation of MOZART, version 2, J. Geophys. Res., 108, 4784–4813, http://dx.doi.org/10.1029/2002JD002853, 2003.

Huijnen, V., Williams, J., van Weele, M., van Noije, T., Krol, M., Dentener, F., Segers, A., Houweling, S., Peters, W., de Laat, J., Boersma, F., Bergamaschi, P., van Velthoven, P., Le Sager, P., Eskes, H.,

Alkemade, F., Scheele, R., Nedelec, P., and Paetz, H. . W.: The global chemistry transport model TM5: description and evaluation of the tropospheric chemistry version 3.0, Geoscientific Model Development, 3, 445–473, doi:10.5194/gmd-3-445-2010, 2010.

IPCC: IPCC, Climate Change 2013: The Physical Science Basis. Contributions of working Group 1 to the Fifth Assessment of the IPCC, www.ipcc.ch, International Panel on Climate Change, 2013.

Kaminski, J. W., Neary, L., Struzewska, J., McConnell, J. C., Lupu, A., Jarosz, J., Toyota, K., Gong, S. L., Côté, J., Liu, X., Chance, K., and Richter, A.: GEM-AQ, an on-line global multi-scale chemical weather modelling system: model description and evaluation of gas phase chemistry processes, Atmospheric Chemistry and Physics, 8, 3255–3281, doi:10.5194/acp-8-3255-2008, http://www.atmos-chem-phys.net/8/3255/2008/, 2008.

Lamarque, J. . F., Emmons, L. K., Hess, P. G., Kinnison, D. E., Tilmes, S., Vitt, F., Heald, C. L., Holland, E. A., Lauritzen, P. H., Neu, J., Orlando, J. J., Rasch, P. J., and Tyndall, G. K.: CAM-chem: description and evaluation of interactive atmospheric chemistry in the Community Earth System Model, Geoscientific Model Development, 5, 369–411, doi:10.5194/gmd-5-369-2012, 2012.

Lelieveld, J. and Dentener, F. J.: What controls tropospheric ozone?, J. Geophys. Res., 105, 3531–3551, http://dx.doi.org/10.1029/1999JD901011, 2000.

Liu, S. C., Kley, D., McFarland, M., Mahlman, J. D., and Levy, H.: On the Origin of Tropospheric Ozone, Journal of Geophysical Research-oceans and Atmospheres, 85, 7546–7552, doi:10.1029/JC085iC12p07546, 1980.

Loveland, T. R., Reed, B. C., Brown, J. F., Ohlen, D. O., Zhu, Z., Yang, L., and Merchant, J. W.: Development of a global land cover characteristics database and IGBP DISCover from 1 km AVHRR data, International Journal of Remote Sensing, 21, 1303–1330, doi:10.1080/014311600210191, 2000.

Mikkelsen, T. N., Ro-Poulsen, H., Pilegaard, K., Hovmand, M. F., Jensen, N. O., Christensen, C. S., and Hummelshoej, P.: Ozone uptake by an evergreen forest canopy: temporal variation and possible mechanisms, Environmental Pollution, 109, 423–429, doi:10.1016/S0269-7491(00)00045-2, 2000.

Mikkelsen, T. N., Ro-Poulsen, H., Hovmand, M. F., Jensen, N. O., Pilegaard, K., and Egelov, A. H.: Five-year measurements of ozone fluxes to a Danish Norway spruce canopy, Atmospheric Environment, 38, 2361–2371, doi:10.1016/j.atmosenv.2003.12.036, 2004.

Muller, J. B. A., Percival, C. J., Gallagher, M. W., Fowler, D., Coyle, M., and Nemitz, E.: Sources of uncertainty in eddy covariance ozone flux measurements made by dry chemiluminescence fast response analysers, Atmospheric Measurement Techniques, 3, 163–176, doi:10.5194/amt-3-163-2010, 2010.

Munger, J. W., Wofsy, S. C., Bakwin, P. S., Fan, S. M., Goulden, M. L., Daube, B. C., Goldstein, A. H., Moore, K. E., and Fitzjarrald, D. R.: Atmospheric deposition of reactive nitrogen oxides and ozone in a temperate deciduous forest and a subarctic woodland .1. Measurements and mechanisms, Journal of Geophysical Research-atmospheres, 101, 12 639–12 657, doi:10.1029/96JD00230, 1996.

Pitari, G., Palermi, S., Visconti, G., and Prinn, R. G.: Ozone Response To A Co2 Doubling - Results From A Stratospheric Circulation Model With Heterogeneous Chemistry, Journal of Geophysical Research-atmospheres, 97, 5953–5962, 1992.

Prather, M. J. and Ehhalt, D.: Atmospheric Chemistry and Greenhouse Gases, in Climate Change 2001: The Scientific Basis, Cambridge University Press, 2001.

Rannik, U., Altimir, N., Mammarella, I., Back, J., Rinne, J., Ruuskanen, T. M., Hari, P., Vesala, T., and Kulmala, M.: Ozone deposition into a boreal forest over a decade of observations: evaluating deposition partitioning and driving variables, Atmospheric Chemistry and Physics, 12, 12 165–12 182, doi:10.5194/acp-12-12165-2012, 2012.

Reich, P. B. and Amundson, R. G.: Ambient Levels of Ozone Reduce Net Photosynthesis In Tree and Crop Species, Science, 230, 566–570, doi:10.1126/science.230.4725.566, 1985.

Rotman, D. A., Tannahill, J. R., Kinnison, D. E., Connell, P. S., Bergmann, D., Proctor, D., Rodriguez, J. M., Lin, S. J., Rood, R. B., Prather, M. J., Rasch, P. J., Considine, D. B., Ramaroson, R., and Kawa, S. R.: Global Modeling Initiative assessment model: Model description, integration, and testing of the transport shell, Journal of Geophysical Research-atmospheres, 106, 1669–1691, doi:10.1029/2000JD900463, 2001.

Rotman, D. A., Atherton, C. S., Bergmann, D. J., Cameron-Smith, P. J., Chuang, C. C., Connell, P. S., Dignon, J. E., Franz, A., Grant, K. E., Kinnison, D. E., Molenkamp, C. R., Proctor, D. D., and Tannahill, J. R.: IMPACT, the LLNL 3-D global atmospheric chemical transport model for the combined troposphere and stratosphere: Model description and analysis of ozone and other trace gases, Journal of Geophysical Research-atmospheres, 109, D04 303, doi:10.1029/2002JD003155, 2004.

Rummel, U., Ammann, C., Kirkman, G. A., Moura, M. A. L., Foken, T., Andreae, M. O., and Meixner, F. X.: Seasonal variation of ozone deposition to a tropical rain forest in southwest Amazonia, Atmospheric Chemistry and Physics, 7, 5415–5435, 2007.

Sanderson, M. G., Dentener, F. J., Fiore, A. M., Cuvelier, C., Keating, T. J., Zuber, A., Atherton, C. S., Bergmann, D. J., Diehl, T., Doherty, R. M., Duncan, B. N., Hess, P., Horowitz, L. W., Jacob, D. J., Jonson, J. . E., Kaminski, J. W., Lupu, A., MacKenzie, I. A., Mancini, E., Marmer, E., Park, R., Pitari, G., Prather, M. J., Pringle, K. J., Schroeder, S., Schultz, M. G., Shindell, D. T., Szopa,

30

S., Wild, O., and Wind, P.: A multi-model study of the hemispheric transport and deposition of oxidised nitrogen, Geophysical Research Letters, 35, L17 815, doi:10.1029/2008GL035389, 2008.

Shindell, D. T., Grenfell, J. L., Rind, D., Grewe, V., and Price, C.: Chemistry-climate interactions in the Goddard Institute for Space Studies general circulation model: 1. Tropospheric chemistry model description and evaluation, J. Geophys. Res., 106, 8047–8075, http://dx.doi.org/10.1029/2000JD900704, 2001.

Simpson, D.: Long-period Modeling of Photochemical Oxidants In Europe - Model-calculations For July 1985, Atmospheric Environment Part A-general Topics, 26, 1609–1634, doi:10.1016/0960-1686(92)90061-O, 1992.

Simpson, D., Benedictow, A., Berge, H., Bergstrom, R., Emberson, L. D., Fagerli, H., Flechard, C. R., Hayman, G. D., Gauss, M., Jonson, J. E., Jenkin, M. E., Nyiri, A., Richter, C., Semeena, V. S., Tsyro, S., Tuovinen, J. . P., Valdebenito, A., and Wind, P.: The EMEP MSC-W chemical transport model - technical description, Atmospheric Chemistry and Physics, 12, 7825–7865, doi:10.5194/acp-12-7825-2012, 2012.

Simpson, D., Arneth, A., Mills, G., Solberg, S., and Uddling, J.: Ozone — the persistent menace: interactions with the N cycle and climate change, Current Opinion in Environmental Sustainability, 9–10, 9 – 19, doi:http://dx.doi.org/10.1016/j.cosust.2014.07.008, http://www.sciencedirect.com/science/article/pii/S1877343514000414, sI: System dynamics and sustainability, 2014.

Sitch, S., Cox, P. M., Collins, W. J., and Huntingford, C.: Indirect radiative forcing of climate change through ozone effects on the land-carbon sink, Nature, 448, 791–U4, doi:10.1038/nature06059, 2007.

Stella, P., Personne, E., Loubet, B., Lamaud, E., Ceschia, E., Beziat, P., Bonnefond, J. M., Irvine, M., Keravec, P., Mascher, N., and Cellier, P.: Predicting and partitioning ozone fluxes to maize crops from sowing to harvest: the Surfatm-O-3 model, Biogeosciences, 8, 2869–2886, doi:10.5194/bg-8-2869-2011, 2011.

Stevenson, D. S., Dentener, F. J., Schultz, M. G., Ellingsen, K., van Noije, T. P. C., Wild, O., Zeng, G., Amann, M., Atherton, C. S., Bell, N., Bergmann, D. J., Bey, I., Butler, T., Cofala, J., Collins, W. J., Derwent, R. G., Doherty, R. M., Drevet, J., Eskes, H. J., Fiore, A. M., Gauss, M., Hauglustaine, D. A., Horowitz, L. W., Isaksen, I. S. A., Krol, M. C., Lamarque, J. F., Lawrence, M. G., Montanaro, V., Muller, J. F., Pitari, G., Prather, M. J., Pyle, J. A., Rast, S., Rodriguez, J. M., Sanderson, M. G., Savage, N. H., Shindell, D. T., Strahan, S. E., Sudo, K., and Szopa, S.: Multimodel ensemble

simulations of present-day and near-future tropospheric ozone, Journal of Geophysical Research-atmospheres, 111, D08 301, doi:10.1029/2005JD006338, 2006.

Sudo, K., Takahashi, M., Kurokawa, J.-i., and Akimoto, H.: CHASER: A global chemical model of the troposphere 1. Model description, J. Geophys. ;Res., 107, 4339–4359, http://dx.doi.org/10.1029/2001JD001113, 2002.

Tai, A. P. K., Martin, M. V., and Heald, C. L.: Threat to future global food security from climate change and ozone air pollution, Nature Climate Change, 4, 817–821, doi:10.1038/NCLIMATE2317, 2014.

The Royal Society: Ground-level ozone in the 21st century: future trends, impacts and policy implications, Policy Document, 15/08, 2008.

Tuovinen, J. P., Ashmore, M. R., Emberson, L. D., and Simpson, D.: Testing and improving the EMEP ozone deposition module, Atmospheric Environment, 38, UNECE, doi:10.1016/j.atmosenv.2004.01.026, 2004.

Tuovinen, J.-P., Emberson, L., and Simpson, D.: Modelling ozone fluxes to forests for risk assessment: status and prospects, Annals of Forest Science, 66, 401, doi:10.1051/forest/2009024, 2009.

ValMartin, M., Heald, C. L., and Arnold, S. R.: Coupling dry deposition to vegetation phenology in the Community Earth System Model: Implications for the simulation of surface O3, Geophysical Research Letters, 41, 2988–2996, doi:10.1002/2014GL059651, http://dx.doi.org/10.1002/2014GL059651, 2014.

Van Dingenen, R., Dentener, F. J., Raes, F., Krol, M. C., Emberson, L., and Cofala, J.: The global impact of ozone on agricultural crop yields under current and future air quality legislation, Atmospheric Environment, 43, 604–618, doi:10.1016/j.atmosenv.2008.10.033, 2009.

Wang, Y. H., Jacob, D. J., and Logan, J. A.: Global simulation of tropospheric O-3-NOx-hydrocarbon chemistry 1. Model formulation, Journal of Geophysical Research-atmospheres, 103, 10 713–10 725, doi:10.1029/98JD00158, 1998.

Wesely, M. L.: Parameterization of Surface Resistances To Gaseous Dry Deposition In Regional-scale Numerical-models, Atmospheric Environment, 23, 1293–1304, doi:10.1016/0004-6981(89)90153-4, 1989.

Wesely, M. L. and Hicks, B. B.: A review of the current status of knowledge on dry deposition, Atmospheric Environment, 34, 2261–2282, doi:10.1016/S1352-2310(99)00467-7, 2000.

WHO: WHO Air quality guidelines for particulate matter, ozone, nitrogen dioxide, and sulfur dioxde. Global update 2005. Summary of risk assessment, Tech. rep., World Health Organisation, WHO Press, World Health Organization, 20 Avenue Appia, 1211 Geneva 27, Switzerland, 2005.

Wild, O.: Modelling the global tropospheric ozone budget: exploring the variability in current models, Atmospheric Chemistry and Physics, 7, 2643–2660, 2007.

Wild, O. and Prather, M. J.: Excitation of the primary tropospheric chemical mode in a global three-dimensional model, J. Geophys. Res., 105, 24 647–24 660, http://dx.doi.org/10.1029/2000JD900399, 2000.

Wolfe, G. M., Thornton, J. A., McKay, M., and Goldstein, A. H.: Forest-atmosphere exchange of ozone: sensitivity to very reactive biogenic VOC emissions and implications for in-canopy photochemistry, Atmospheric Chemistry and Physics, 11, 7875–7891, doi:10.5194/acp-11-7875-2011, 2011.

Wu, S., Mickley, L. J., Kaplan, J. O., and Jacob, D. J.: Impacts of changes in land use and land cover on atmospheric chemistry and air quality over the 21st century, Atmospheric Chemistry and Physics, 12, 1597–1609, doi:10.5194/acp-12-1597-2012, 2012.

Young, P. J., Archibald, A. T., Bowman, K. W., Lamarque, J. . F., Naik, V., Stevenson, D. S., Tilmes, S., Voulgarakis, A., Wild, O., Bergmann, D., Cameron-Smith, P., Cionni, I., Collins, W. J., Dalsoren, S. B., Doherty, R. M., Eyring, V., Faluvegi, G., Horowitz, L. W., Josse, B., Lee, Y. H., MacKenzie, I. A., Nagashima, T., Plummer, D. A., Righi, M., Rumbold, S. T., Skeie, R. B., Shindell, D. T., Strode, S. A., Sudo, K., Szopa, S., and Zeng, G.: Pre-industrial to end 21st century projections of tropospheric ozone from the Atmospheric Chemistry and Climate Model Intercomparison Project (ACCMIP), Atmospheric Chemistry and Physics, 13, 2063–2090, doi:10.5194/acp-13-2063-2013, 2013.

Zeng, T., Wang, Y. H., Chance, K., Browell, E. V., Ridley, B. A., and Atlas, E. L.: Widespread persistent near-surface ozone depletion at northern high latitudes in spring, Geophysical Research Letters, 30, 2298, doi:10.1029/2003GL018587, 2003.

Zhang, L. M., Moran, M. D., Makar, P. A., Brook, J. R., and Gong, S. L.: Modelling gaseous dry deposition in AURAMS: a unified regional air-quality modelling system, Atmospheric Environment, 36, 537–560, doi:10.1016/S1352-2310(01)00447-2, 2002.

Table 1. Summary of the deposition schemes and annual total global O_3 dry deposition fluxes for 15 TF HTAP models.

Model	Deposition Scheme[a]	Land Cover Classes[b]	Annual global O_3 deposition / Tg yr^{-1}	Reference
CAMCHEM-3311m13	Wesely	17	861	Lamarque et al. (2012)
CAMCHEM-3514	Wesely	17	818	Lamarque et al. (2012)
CHASER-v03	Wesely		939	Sudo et al. (2002)
FRSGC/UCI-v01	Wesely	9	943	Wild and Prather (2000)
GEMAQ-EC	Wesely	15	878	Kaminski et al. (2008)
GEOSChem-v07	Wesely	11	913	Bey et al. (2001)
GISS-PUCCINI-modelA	Wesely	8	975	Shindell et al. (2001)
GISS-PUCCINI-modelEaer	Wesely	8	1112	Shindell et al. (2001)
GISS-PUCCINI-modelE	Wesely	8	1179	Shindell et al. (2001)
GMI-v02f	Wesely		819	Rotman et al. (2001)
INCA-vSSz	Wesely	11	1256	Hauglustaine et al. (2004)
LLNL-IMPACT-T5a	Wesely	13	1000	Rotman et al. (2004)
MOZARTGFDL-v2	Wesely	11	997	Horowitz et al. (2003)
STOC-HadAM3-v01	Wesely	9	1095	Collins et al. (2003)
STOCHEM-v02	Wesely	9	834	Collins et al. (1997)
TM5-JRC-cy2-ipcc-v1	Wesely	4	844	Huijnen et al. (2010)
ULAQ-v02	Prescribed[c]		1116	Pitari et al. (1992)
UM-CAM-v01	Prescribed[c]	5	1023	Zeng et al. (2003)
Average ($\pm 1\sigma$)			978 ± 127	
Average seasonal amplitude[d]			38 ± 8	
Average monthly range[e]			38 ± 6	

[a] The Wesely scheme has been updated from the orginal scheme (Wesely, 1989) in many of these models. Further details about these updates are given in the supplementary information.

[b] The number of land cover classes used in the model are shown here. The land cover classes are listed for each model in the supplementary information.

[c] Deposition velocities are prescribed for land cover type, season and whether it is day or night.

[d] Defined here as the difference in total global O_3 dry deposition between the months with highest and lowest deposition fluxes.

[e] Average monthly range is the average spread across the models for each month.

Table 2. Land cover classification for the OW11 and GLCF data sets.

Land cover class		Abbreviation		% Area	
OW11	GLCF	OW11	GLCF	OW11	GLCF
Snow and Ice	Snow and Ice	SI	SI	2.7	3.5
Deciduous Forest	Broadleaf Deciduous Forest	DF	BD	4.9	0.7
–	High Latitude Deciduous Forest	–	HL	–	1.2
Coniferous Forest	Coniferous Evergreen Forest	CF	CE	3.1	2.5
–	Mixed Coniferous Forest and Woodland	–	MC	–	1.4
Agricultural Land, Crops	Crops	AC	CR	2.7	3.1
Grassland	Grassland	GL	GL	8.2	4.3
–	Wooded Grassland	–	WG	–	4.7
Tropical Forest	Broadleaf Evergreen Forest	TF	BE	0.8	2.9
Tundra	Tundra	TN	TN	1.7	1.5
Desert	Bare ground	DT	BG	3.8	3.4
–	Shrubs, Bare Ground	–	SB	–	2.1
Wetland	–	WL	–	0.7	–
Urban	–	UB	–	0.0	–
Water	Water	WT	WT	71.2	68.6
Total				100	100

Table 3. O_3 dry deposition measurement sites.

Site Name	Grid Reference	Landcover	Sampling Height / m	LAI	Sampling Period	Reference
Long term sites						
Ulborg (Denmark)	56°17′ N 8°25′ E	Mixed coniferous forest	18, 36	8	Oct 1995–Dec 2000	Mikkelsen et al. (2004, 2000)
Castel Porziano (Italy)	41°44′ N 12°24′ E	Holm Oak forest	35	4.76	Jan 2013–Dec 2013	Fares et al. (2014)
Auchencorth Moss (Scotland)	55°47′ N 3°14′ W	Moorland	0.3–3.0	na[a]	Jan 1995–Dec 1998	Fowler et al. (2001)
Hyytiala (Finland)	61°51′ N 24°17′ E	Scots Pine forest	23	6–8	Jan 2002–Dec 2003	Rannik et al. (2012)
Harvard Forest (MA, USA)	42°32′ N 72°11′ W	Mixed deciduous forest	30	3.4	Jan 1992–Dec 2001	Munger et al. (1996)
Citrus orchard (CA, USA)	36°21′ N 119°5′ W	Citrus orchard	1.0–9.2	3.0	Oct 2009–Nov 2010	Fares et al. (2012)
Blodgett Forest (CA, USA)	38°53′ N 120°37′ W	Pine plantation	12.5	1.2–2.9	Jan 2001–Dec 2007	Fares et al. (2010)
Short term sites						
Danum Valley (Borneo)	4°58′ N 117°51′ E	Tropical forest	75	6	Apr, Jul 2008	Fowler et al. (2011)
Sabahmas (Borneo)	5°15′ N 118°27′ E	Oil palm	15	6	Apr 2008	Fowler et al. (2011)
South West Amazon (Brazil)	3° S 60° W	Tropical forest	53	5.6	May 1999 Sep–Oct 1999	Rummel et al. (2007)
Central Amazon (Brazil)	10°5′ N 61°55′ W	Tropical forest	39		Apr–May 1987	Fan et al. (1990)
Grignon (France)	48°51′ N 1°58′ E	Maize crop	3.4, 6.4, 3.7	5.3–3.6	Ap 2008–Sep2008	Stella et al. (2011)
La Cape Sud (France)	44°24′ N 0°38′ E	Maize crop	3.4, 6.4, 3.7	5.1	Jul 2007–Oct2007	Stella et al. (2011)
Lamasquere (France)	43°49′ N 1°23′ E	Maize crop	3.4, 6.4, 3.7	3.2	May 2008–Sep 2008	Stella et al. (2011)
Castel Porziano[b] (Italy)	41°43′ N 12°23′ E	Pseudo-steppe	8, 2	na	Jun 1993, May 1994	Cieslik and Labatut (1997)
Burriana (Spain)	39°55′ N 0°03′ W	Citrus orchard	10	na	16–29 Jul 1995 28 Apr–3 May 1996	Cieslik (2004)
Voghera (Italy)	45°01′ N 9°00′ E	Onion field	2.5	na	May–Jul 2003	Gerosa et al. (2007)
Le Dezert (France)	44°05′ N 0°43′ E	Pine forest	37	na	16–18 Apr 1997	Cieslik (2004)
Klippeneck (Germany)	48°10′ N 8°45′ E	Grass	2, 8	na	10–22 Sep 1992	Cieslik (2004)
San Pietro Capofiume (Italy)	44°39′ N 11°37′ E	Beet crop	8	na	15–22 Jun 1993	Cieslik (2004)
Viols en Levant (France)	43°41′ N 3°47′ E	Mediterranean shrub	37	na	16–24 Jul 1998	Cieslik (2004)
Gilchriston Farm (Scotland)	56° N 3° E	Potato crop	2.2	na	Jul	Coyle et al. (2009)

[a] na: The data were not reported in the study.
[b] The short term measurements made at Castel Porziano were part of a different campaign from the long term data set and were made at a different location.
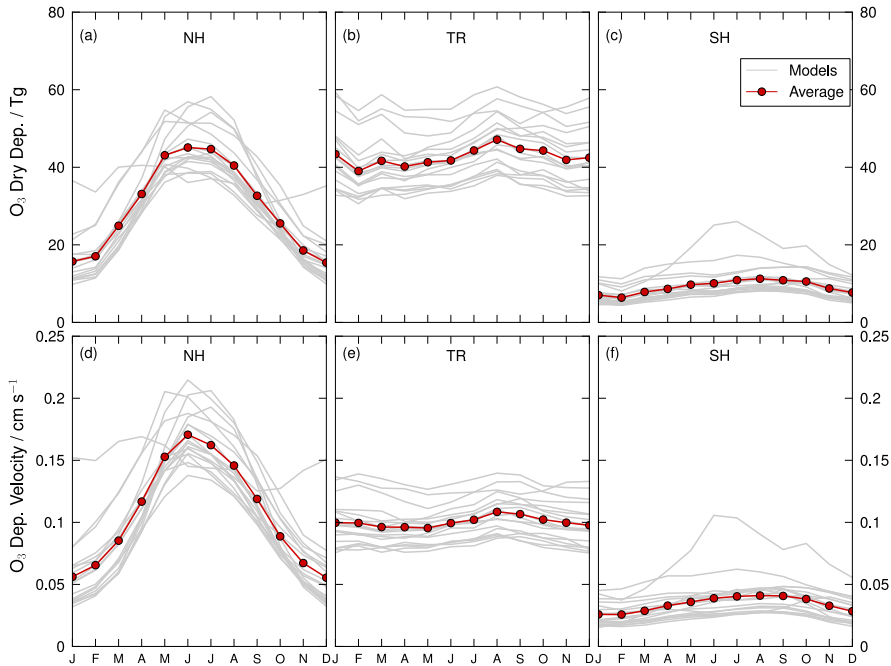
38

Figure 1. Total monthly O$_3$ dry deposition (top, **a–c**) and monthly average O$_3$ deposition velocity (bottom, **d–f**) for 15 models participating in the TF HTAP model intercomparison project. Modelled monthly total O$_3$ dry deposition is shown for the Northern Hemisphere extra-Tropics 30°–90° N (**a, d**), Tropics 30° N–30° S (**b, e**), and Southern Hemisphere extra-Tropics 30°–90° S (**c, f**).
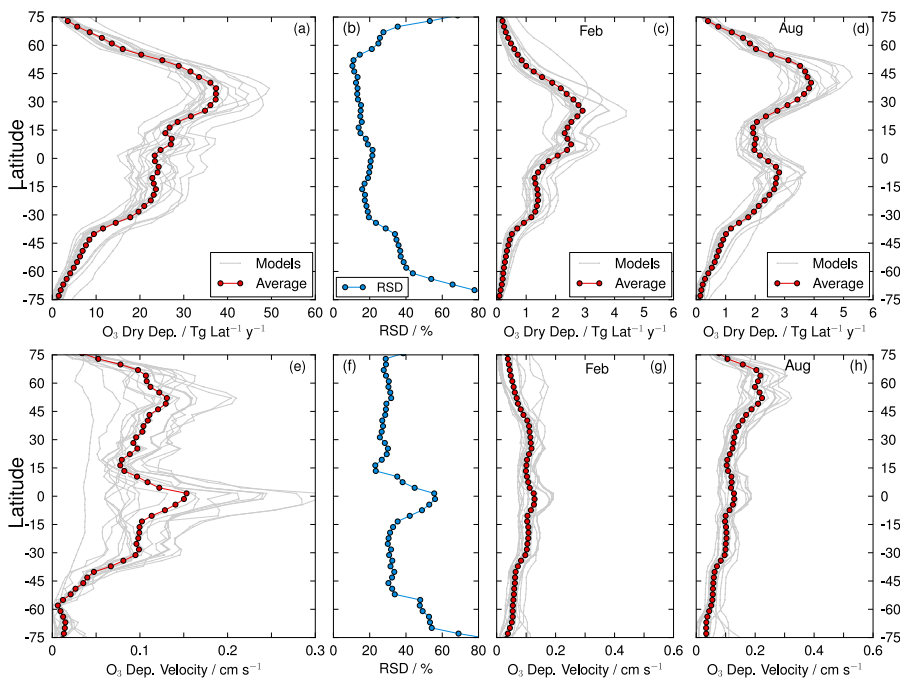
Figure 2. Latitudinal distribution of total O_3 dry deposition (top row) and average O_3 deposition velocities (bottom row) per $3°$ latitude band for the model ensemble. Panels show the total annual O_3 dry deposition and average annual O_3 dry deposition velocity **(a, e)**, the relative standard deviation (RSD) in annual deposition and average annual deposition velocity across the models **(b, f)**, and the total monthly O_3 dry deposition fluxes and average annual dry deposition velocities in February **(c, g)** and August **(d, h)**.
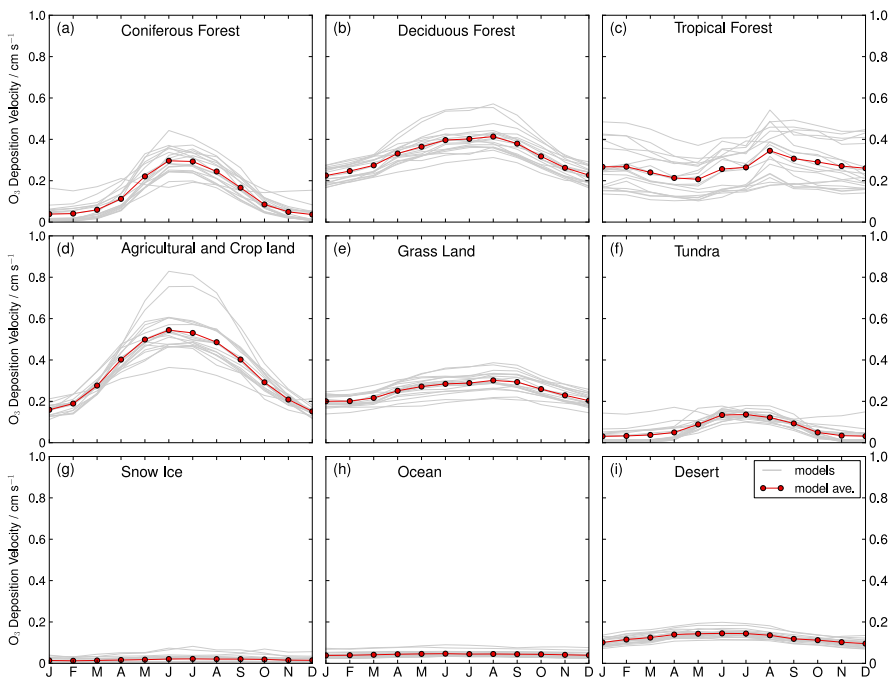
Figure 3. Average monthly O_3 dry deposition velocities at grid cells with 100% coverage of a given land cover class. Model deposition velocities are shown in grey and the ensemble average in red.
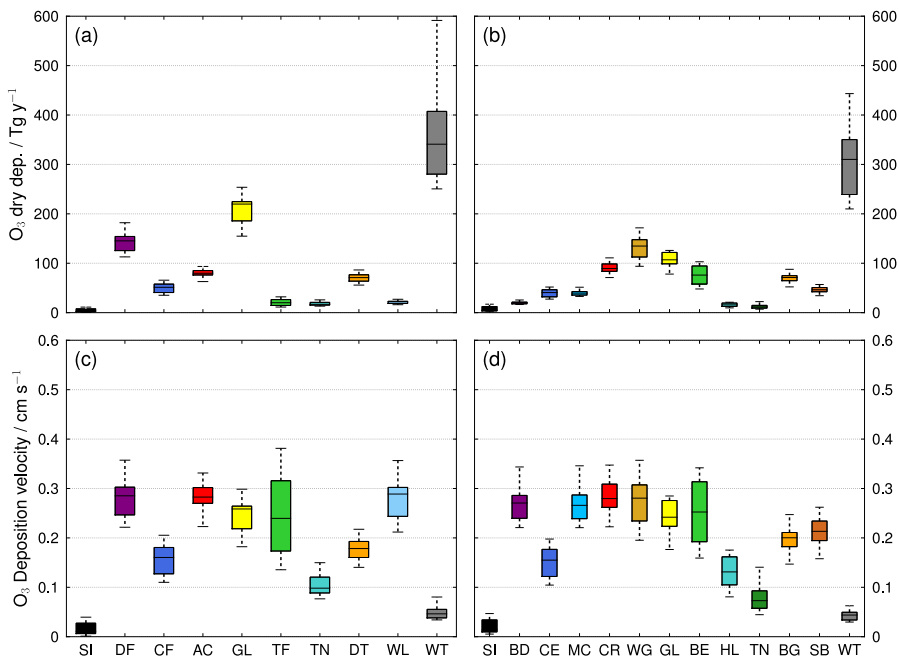
Figure 4. Total annual O_3 dry deposition and annual average O_3 deposition velocity partitioned to land cover classes using the OW11 **(a, c)** and GLCF **(b, d)** datasets. Upper panels show the contribution of each LCC to the global annual O_3 dry deposition flux, and lower panels show the average deposition velocity to each LCC. The box and whiskers for each land class represent the median, quartiles and 10th/90th percentiles over the 15 contributing models.
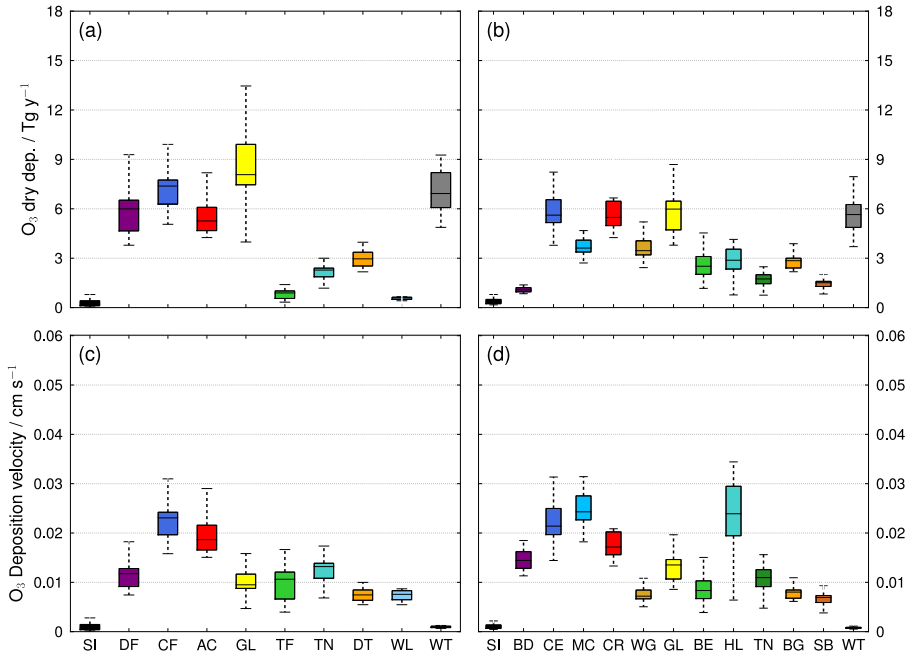
Figure 5. Seasonal amplitude in total global O_3 dry deposition partitioned to the OW11 **(a)** and GLCF **(b)** land cover classes. The monthly range in average O_3 dry deposition velocity is shown in the lower panels for OW11 **(c)** and GCLF **(d)** land cover classes. The box and whiskers represent the median, quartiles and 10th/90th percentiles over the model ensemble.
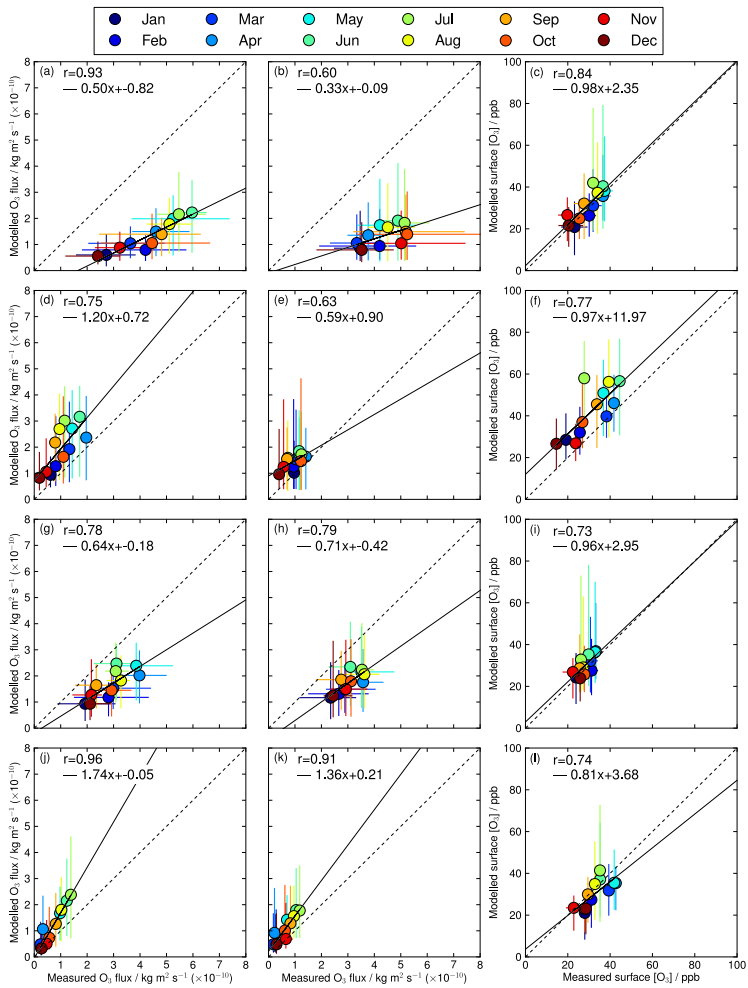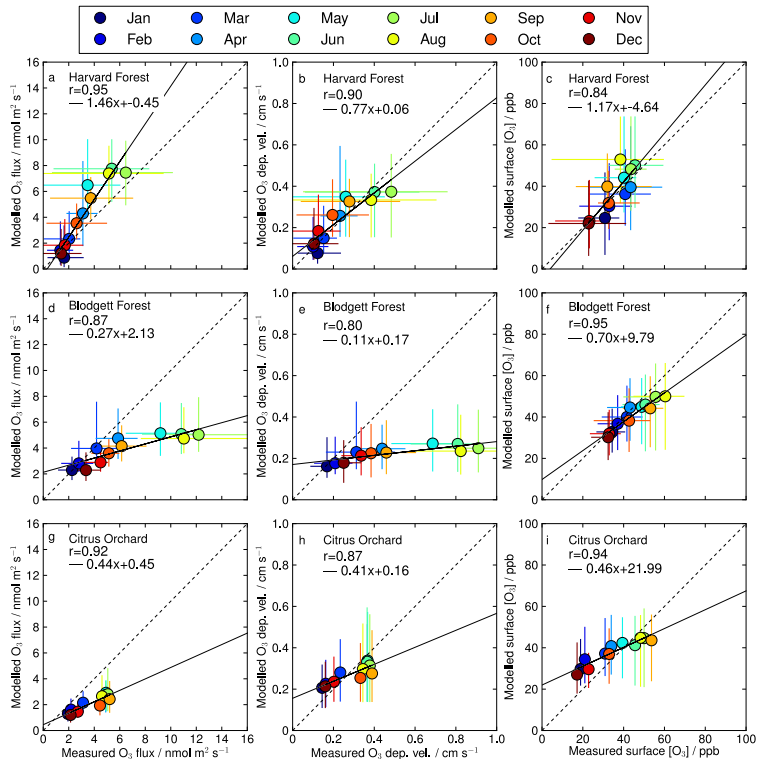
Figure 6. Comparison of observed and modelled monthly average O_3 dry deposition fluxes, O_3 dry deposition velocities and surface O_3 at European measurement sites. Individual sites are shown by row for Ulborg **(a–c)**, Hyytiala **(d–f)**, Castel Porziano **(g–i)** and Auchencorth Moss **(j–l)**. Observed and modelled fluxes at each site are compared directly in the left hand column, deposition velocities are shown in the middle column, and surface O_3 is compared in the right hand column. Vertical bars represent the range across the models and horizontal bars represent the interannual range in the observations, where available.

Figure 7. Comparison of observed and modelled monthly average O_3 dry deposition fluxes, O_3 dry deposition velocities and surface O_3 at North American measurement sites. Individual sites are shown by row for Harvard Forest **(a–c)**, Blodgett Forest **(d–f)** and Californian Citrus Orchard **(g–i)**. Observed and modelled fluxes at each site are compared directly in the left hand column, deposition velocities are shown in the middle column, and surface O_3 is compared in the right hand column. Vertical bars represent the range across the models and horizontal bars represent the interannual range in the observations, where available.
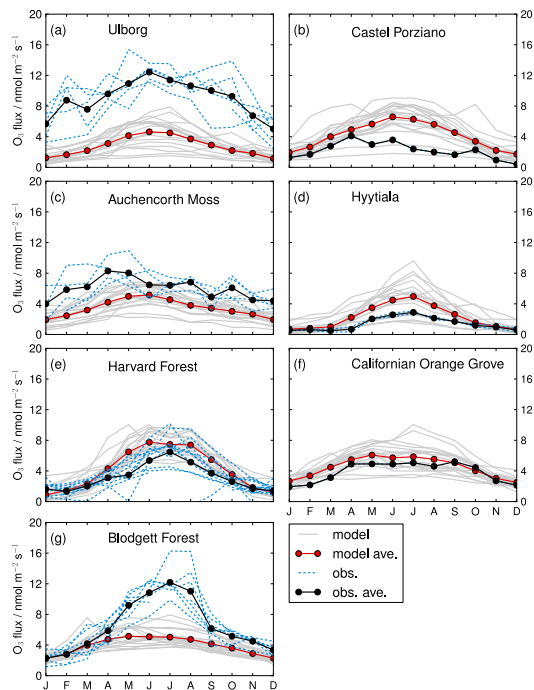
Figure 8. Measured and modelled monthly average O_3 dry deposition fluxes at Ulborg **(a)**, Castel Porziano **(b)**, Auchencorth Moss **(c)**, Hyytiala **(d)**, Harvard Forest **(e)**, Californian citrus orchard **(f)**, and Blodgett Forest **(g)**. Grey lines show results from individual models and blue lines show observations for different years.
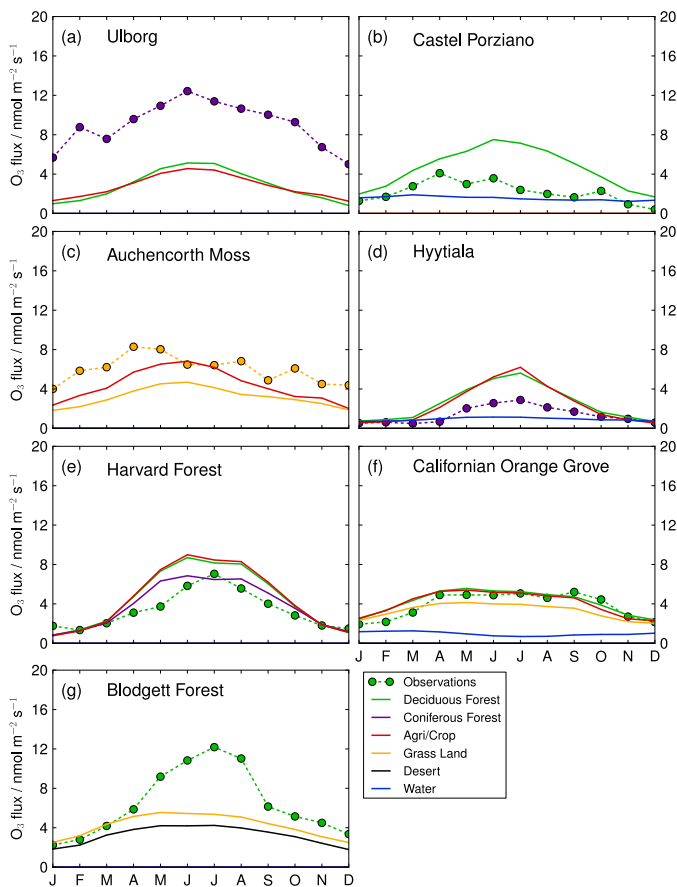
Figure 9. Observed monthly average O_3 dry deposition fluxes at measurement sites (dashed lines) and repartitioned model fluxes for each land cover class (solid lines). Colours indicate the LCC at the site and in the model grid cell containing the site.
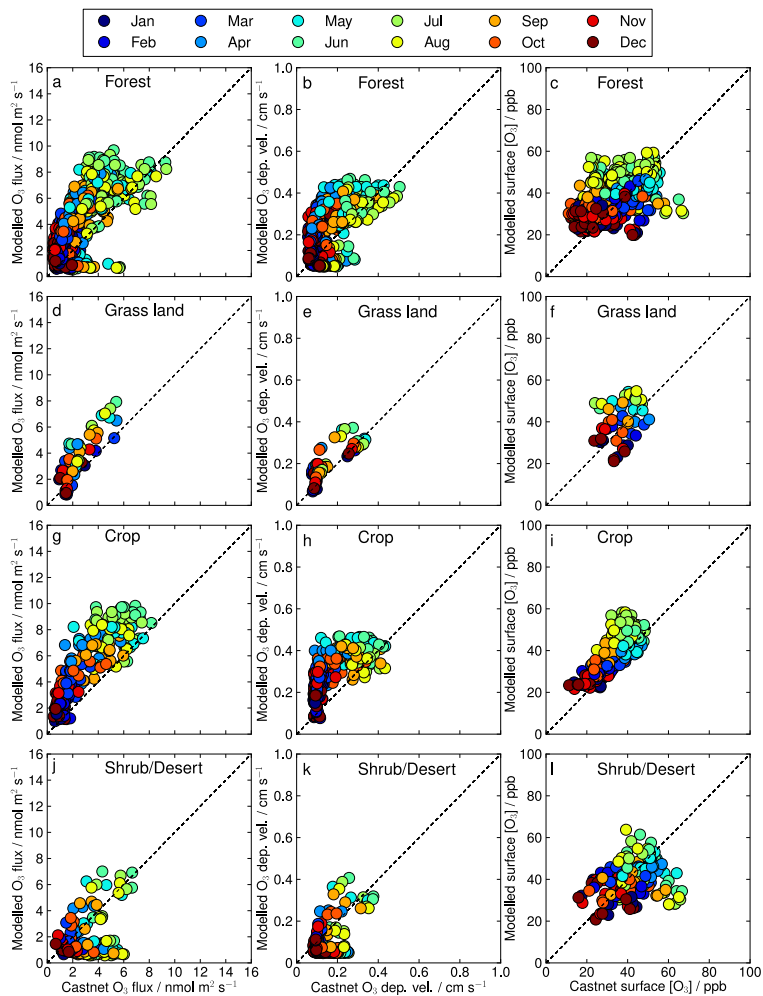
Figure 10. Comparison of CASTNET and modelled monthly average O_3 dry deposition fluxes, O_3 dry deposition velocities and surface O_3 at CASTNET measurement sites. The CASTNET sites are grouped by land cover class which are shown by row for forest sites **(a–c)**, grassland sites **(d–f)**, crop sites **(g–i)** and shrub/desert sites (j–l). CASTNET and modelled fluxes at each site are compared in the left hand column, deposition velocities are shown in the middle column, and surface O_3 is compared in the right hand column.
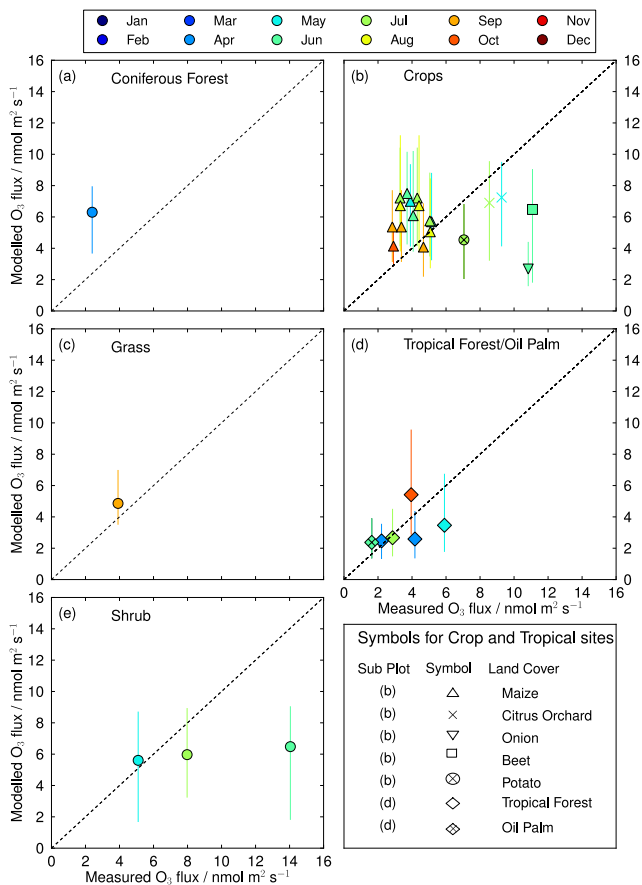
Figure 11. Measured and modelled monthly average O_3 dry deposition fluxes at short-term measurement sites. Colours indicated the average flux for the relevant month and shapes indicate the measurement site.